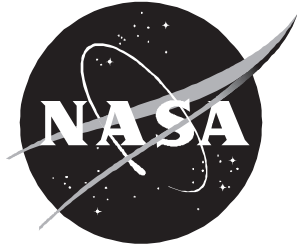


NASA/TP-1998-206938



# Redesign of a Variable-Gain Output Feedback Longitudinal Controller Flown on the High-Alpha Research Vehicle (HARV)

*Aaron J. Ostroff*  
*Langley Research Center, Hampton, Virginia*

---

March 1998

## ***The NASA STI Program Office . . . in Profile***

Since its founding, NASA has been dedicated to the advancement of aeronautics and space science. The NASA Scientific and Technical Information (STI) Program Office plays a key part in helping NASA maintain this important role.

The NASA STI Program Office is operated by Langley Research Center, the lead center for NASA's scientific and technical information. The NASA STI Program Office provides access to the NASA STI Database, the largest collection of aeronautical and space science STI in the world. The Program Office is also NASA's institutional mechanism for disseminating the results of its research and development activities. These results are published by NASA in the NASA STI Report Series, which includes the following report types:

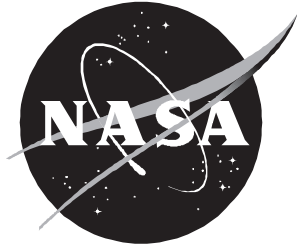
- **TECHNICAL PUBLICATION.** Reports of completed research or a major significant phase of research that present the results of NASA programs and include extensive data or theoretical analysis. Includes compilations of significant scientific and technical data and information deemed to be of continuing reference value. NASA counter-part or peer-reviewed formal professional papers, but having less stringent limitations on manuscript length and extent of graphic presentations.
- **TECHNICAL MEMORANDUM.** Scientific and technical findings that are preliminary or of specialized interest, e.g., quick release reports, working papers, and bibliographies that contain minimal annotation. Does not contain extensive analysis.
- **CONTRACTOR REPORT.** Scientific and technical findings by NASA-sponsored contractors and grantees.
- **CONFERENCE PUBLICATION.** Collected papers from scientific and technical conferences, symposia, seminars, or other meetings sponsored or co-sponsored by NASA.
- **SPECIAL PUBLICATION.** Scientific, technical, or historical information from NASA programs, projects, and missions, often concerned with subjects having substantial public interest.
- **TECHNICAL TRANSLATION.** English-language translations of foreign scientific and technical material pertinent to NASA's mission.

Specialized services that help round out the STI Program Office's diverse offerings include creating custom thesauri, building customized databases, organizing and publishing research results . . . even providing videos.

For more information about the NASA STI Program Office, see the following:

- Access the NASA STI Program Home Page at ***<http://www.sti.nasa.gov>***
- Email your question via the Internet to [help@sti.nasa.gov](mailto:help@sti.nasa.gov)
- Fax your question to the NASA Access Help Desk at (301) 621-0134
- Phone the NASA Access Help Desk at (301) 621-0390
- Write to:  
NASA Access Help Desk  
NASA Center for AeroSpace Information  
800 Elkridge Landing Road  
Linthicum Heights, MD 21090-2934

NASA/TP-1998-206938



# Redesign of a Variable-Gain Output Feedback Longitudinal Controller Flown on the High-Alpha Research Vehicle (HARV)

*Aaron J. Ostroff*  
*Langley Research Center, Hampton, Virginia*

National Aeronautics and  
Space Administration

Langley Research Center  
Hampton, Virginia 23681-2199

---

March 1998

## Acknowledgments

The author wishes to acknowledge the following individuals who made special contributions to the research described in this paper: Keith D. Hoffler, ViGYAN Inc., Hampton, VA, who organized the target tracking maneuvers, supported the motion-based simulation, and supported the research flight tests; Dr. Barton J. Bacon, Langley Research Center, who developed and modified some of the tools used for the analysis; Keith D. Wichman, Dryden Flight Research Center, who supplied the Neal-Smith analysis tool, and who also supported both the motion-base simulation and research flight tests; and James W. Smolka, Dryden Flight Research Center, who served as the pilot for the motion-based simulation research and was one of the project pilots for the research flight tests.

The use of trademarks or names of manufacturers in this report is for accurate reporting and does not constitute an official endorsement, either expressed or implied, of such products or manufacturers by the National Aeronautics and Space Administration.

---

Available from the following:

NASA Center for AeroSpace Information (CASI)  
800 Elkridge Landing Road  
Linthicum Heights, MD 21090-2934  
(301) 621-0390

National Technical Information Service (NTIS)  
5285 Port Royal Road  
Springfield, VA 22161-2171  
(703) 487-4650

**Contents**

Summary . . . . . 1

Introduction . . . . . 1

Symbols . . . . . 2

High-Alpha Research Vehicle (HARV) Description . . . . . 4

Controller Description . . . . . 4

    Baseline Flight Controller . . . . . 4

        Feed-forward controller . . . . . 6

        Feedback controller . . . . . 7

    Modified Controller. . . . . 7

Linear Models . . . . . 9

    Feedback Controller . . . . . 10

    Feed-Forward Controllers . . . . . 12

        Modified controller . . . . . 12

        Baseline controller . . . . . 12

    Closed-Loop Feedback Model . . . . . 13

Linear Analysis . . . . . 13

    Single-Loop Bode Analysis . . . . . 14

    Loop Transfer . . . . . 14

    Structured Singular Value Analysis . . . . . 14

    Neal-Smith Analysis . . . . . 15

    Bode Envelope Criteria . . . . . 19

Piloted Simulation . . . . . 21

    Facility Description . . . . . 21

    Simulation Study . . . . . 21

    Simulation Results . . . . . 23

Flight Results Summary . . . . . 25

Conclusions . . . . . 26

Appendix—Variable-Gain Components and Modified Stochastic Weights . . . . . 28

    Variable-Gain Components . . . . . 28

    Modified Stochastic Weights . . . . . 28

References . . . . . 30

## Summary

This paper describes a redesigned longitudinal controller that flew on the High-Alpha Research Vehicle (HARV) during calendar years (CY) 1995 and 1996. Linear models are developed for both the modified controller and a baseline controller that was flown in CY 1994. The modified controller was developed with three gain sets for flight evaluation, and several linear analysis results are shown comparing the gain sets. A Neal-Smith flying qualities analysis shows that performance for the low- and medium-gain sets is near the level 1 boundary, depending upon the bandwidth assumed, whereas the high-gain set indicates a sensitivity problem. A newly developed high-alpha Bode envelope criterion indicates that the control system gains may be slightly high, even for the low-gain set. A large motion-base simulator in the United Kingdom was used to evaluate the various controllers. Desired performance, which appeared to be satisfactory for flight, was generally met with both the low- and medium-gain sets. Both the high-gain set and the baseline controller were very sensitive, and it was easy to generate pilot-induced oscillation (PIO) in some of the target-tracking maneuvers. Flight target-tracking results varied from level 1 to level 3 and from no sensitivity to PIO. These results were related to pilot technique and whether actuator rate saturation was encountered.

## Introduction

During spring and summer calendar year (CY) 1994, two NASA research flight controllers were flown on the High-Alpha Research Vehicle (HARV). To maximize flight experiment time, one controller was designed for the longitudinal axis and the second controller for the lateral-directional axes. The longitudinal controller methodology is called variable-gain output feedback (refs. 1 through 4) and is the controller that is discussed in this paper. The lateral-directional methodology (ref. 4) is called CRAFT and was combined with a pseudo controls blending approach.

The Variable-Gain methodology (ref. 1) was developed to overcome shortcomings of the traditional approach to gain scheduling. In the traditional approach, constant-gain feedback control laws are designed individually at many operating points over the flight envelope. These feedback gains are then combined by using a curve-fit technique (interpolation, straight-line approximation, or a least squares fit) to generate a gain schedule for the final control gains. Several schedules are often used and combined when more than one independent variable is involved. Depending upon the curve-fit technique used, stability could become an issue.

Variable gain is an integrated design approach in which all design operating conditions are handled simultaneously, creating a more efficient design process. A gain functional is optimally produced within the design algorithm and consists of measured scaling parameters selected by the designer and associated designed gain-matrix components. Feedback gains are calculated continuously during flight, resulting in a smooth-gain schedule. The control system is guaranteed to be stable at all design operating points. Other features of the methodology include (1) output feedback that allows all dynamics to be included in the design process, (2) optimal control that allows tradeoff between states and controls, (3) stochastic design that allows process noise and sensor noise to be included, and (4) direct digital design for applicability to digital computers. Thirty-nine design flight conditions were used for the flight controller described in this paper (ref. 3).

The HARV provided a test bed to demonstrate high-alpha control methodologies using advanced control effectors. In particular, thrust vectoring was the technology used to allow maneuvering during post-stall. The thrust-vectoring controls were installed on a modified F/A-18 airplane and deflected the thrust to provide pitch and yaw motions. Research on this airplane was part of the High-Alpha Technology Program (HATP) (ref. 5) that included other high-alpha related experiments in technology areas such as propulsion, aerodynamics, loads, sensors, and other advanced control effectors.

There were several guidelines that influenced the control design. Pitch agility was one of the most important longitudinal high-alpha design guidelines. An example pitch-up agility guideline is the

requirement to meet peak angular accelerations and rates within specified time constraints when starting from various initial angles of attack. Additional longitudinal guidelines include pitch-down agility, angle-of-attack regulation during stability axis rolls, gross acquisition, and fine tracking. Initially, high-alpha gross acquisition and fine-tracking simulation tasks did not exist. Experimental cases were developed and installed in the simulator prior to the CY 1994 flights, but after the baseline control design was completed and frozen. In addition, analytical high-alpha design guidelines for gross acquisition and fine tracking were being developed during the baseline controller design phase. When these guidelines became available, they were expressed in terms of classical low-order system parameters which could not be readily used in the design method of reference 1.

One philosophy that influenced the design of the baseline control system was that it is more important to point the airplane's nose toward the opponent for a first shot opportunity than it is to track the opponent for relatively long periods of time. This philosophy may be true for combat with missiles but is probably incorrect for combat with guns. Due to the various reasons described, little emphasis was placed upon fine tracking for the CY 1994 flights. The overall result was a highly agile longitudinal control system that had good angle-of-attack regulation and gross acquisition response but poor target acquisition and fine-tracking capability, and the airplane encountered pilot-induced oscillation (PIO) in flight. Except for high-speed tracking at Mach 0.6 at 3g load factor, all other tracking scenarios were unattainable. Based upon the flight results in CY 1994, it was obvious that the longitudinal controller required modification to achieve satisfactory longitudinal tracking characteristics.

The main objectives of this paper are to document changes to the baseline flight controller and to show some of the analyses applied to the modified controller. The first section of this paper includes a brief description of the HARV. A description is then given of both the baseline flight controller and the modified flight controller. Linear models were developed to analyze the modified controller and are shown in the third section, along with linear models for the baseline controller. Linear analysis applied to the modified controller includes typical feedback analysis and some flying qualities analysis, both of which are described in the fourth section. The fifth section of this paper includes results from a large-amplitude motion-based simulator in the United Kingdom (UK). A summary of the CY 1995 and 1996 target-tracking flight results is included in the final section of this paper and is presented in greater detail in reference 6.

## Symbols

In the following list of symbols, matrices and vectors are shown in boldface; scalars are shown in italics.

$a_i$	constants ( $i = 0,1,2,3$ )
$f_2$	nonlinear function (fig. 3)
$g$	gravity, $g$ units
$\mathbf{H}_{zy}$	matrix relating measurements to integrator states
$\mathbf{K}$	feedback gain matrix
$K_{cgt}$	feed-forward gain connecting $y_{cmd}$ to feedback controller
$K_{F1}$	feed-forward gain for load-factor command
$K_{F2}$	feed-forward gain for alpha command
$K_{ff}$	feed-forward gain in modified controller
$\mathbf{K}_i$	components of total gain matrix ( $i = 0,1,\dots,6$ )
$K_n$	proportional feedback gain for $n_z$ , deg/sec/g
$K_p$	pilot gain, in/deg

$K_q$	proportional feedback gain for $q$
$K_{tr}$	gain representing trim bias in baseline feed-forward controller
$K_u$	control filter feedback gain, $\text{sec}^{-1}$
$\mathbf{K}_y$	proportional feedback gain matrix
$K_z$	integrator feedback gain
$K_\alpha$	proportional feedback gain for $\alpha$ , $\text{sec}^{-1}$
$n_z$	load factor, $g$ units
$n_{z,c}$	load-factor command, $g$ units
$\mathbf{p}$	gain-schedule parameter vector
$Q_c$	impact pressure, $\text{lb/ft}^2$
$q$	pitch rate, $\text{deg/sec}$
$s$	Laplace transform variable
$u$	control input
$u_0$	trim condition for control input
$v_c$	rate command, $\text{deg/sec}$
$\mathbf{x}_c$	state vector in feedback controller
$x_m$	state in feed-forward controller
$y$	general output of nonlinear equation
$y_{cmd}$	command from feed-forward command generator
$y_m$	output from feed-forward controller to feedback controller
$y_{n_z}$	load-factor output, $g$ units
$\mathbf{y}_p$	plant output vector
$y_q$	pitch-rate output, $\text{deg/sec}$
$y_u$	controller position command, $\text{deg}$
$y_z$	integrator output
$y_\alpha$	angle-of-attack output, $\text{deg}$
$y_{1c}$	feed-forward signal in load factor command path
$y_{2c}$	feed-forward signal in alpha command path
$z$	$z$ -transform variable
$\alpha$	angle of attack, $\text{deg}$
$\alpha_c$	angle-of-attack command, $\text{deg}$
$\alpha_{oc}$	angle-of-attack trim command, $\text{deg}$
$\Delta T$	sampling period, 0.0125 sec
$\Delta y$	error in integrator path in feedback controller
$\delta_{sc}$	symmetric stabilator command, $\text{deg}$
$\delta_{sp}$	pilot stick command, in.
$\delta_{vc}$	pitch thrust-vectoring command, $\text{deg}$
$\theta$	pitch attitude, $\text{deg}$
$\theta_e$	pitch attitude tracking error, $\text{deg}$

$\tau_{LAG}$  pilot compensation lag time constant, sec  
 $\tau_{LEAD}$  pilot compensation lead time constant, sec  
 $\tau_p$  pilot time delay, sec  
 $\omega_B$  bandwidth, rad/sec

Subscripts:

$c$  controller or command  
 $k$  coefficient for sampling sequence

Abbreviations:

CGI computer-generated image  
 CHR Cooper-Harper rating  
 CY calendar year  
 DRA Defence Research Agency in United Kingdom  
 FFCG feed-forward command generator  
 HARV High-Alpha Research Vehicle  
 HATP High-Alpha Technology Program  
 PIF proportional integral filter  
 PIO pilot-induced oscillation  
 PIOR pilot-induced oscillation rating

## High-Alpha Research Vehicle (HARV) Description

The HARV configuration is an F/A-18 airplane modified to have multi-axis thrust vectoring for additional pitch and yaw control power. The F/A-18 is a multirole fighter-attack airplane with supersonic dash capability and, by today's standards, exhibits good low-speed high-alpha maneuvering capability. The propulsion system has two General Electric F-404 turbofan engines with afterburners. The secondary (divergent) nozzles of the engines were removed, and thrust-vectoring vanes plus actuators were mounted directly on the airplane structure. Each engine had three hydraulically actuated vanes that were deflected into the engine exhaust plume to vector the thrust and to produce the desired pitching and yawing moments. A mixer was designed (ref. 7) to distribute the pitch and yaw commands from the flight controllers to the six vane actuators. The modified airplane is shown in figure 1. The thrust-vectoring system resulted in additional weight at the rear end of the airplane, and ballast had to be added to the nose of the HARV to maintain the center-of-gravity location. Compared to an unmodified F/A-18, the HARV had increased inertia and was approximately 4000 lb heavier.

## Controller Description

This section contains a description of the baseline flight controller flown in CY 1994 and the modified controller flown in CY 1995 and 1996. Each controller is presented in the following separate subsections. Symbols that follow show matrices and vectors in boldface and scalars in italics.

### Baseline Flight Controller

Figure 2 shows a block diagram of the HARV longitudinal controller containing the main components for the feedback and feed-forward controller designs (ref. 3). Pilot commands  $\delta_{sp}$  are input to the FFCG (feed-forward command generator) which generates  $y_{cmd}$  based upon the automatic selection of either an alpha-command mode  $\alpha_c$  or a load-factor-command mode  $n_{z,c}$ . Output  $y_{cmd}$  goes to both the feed-forward gain  $K_{cgt}$  and to the variable-gain feedback controller, composed of the dynamic feedback



Figure 1. High-Alpha Research Vehicle.

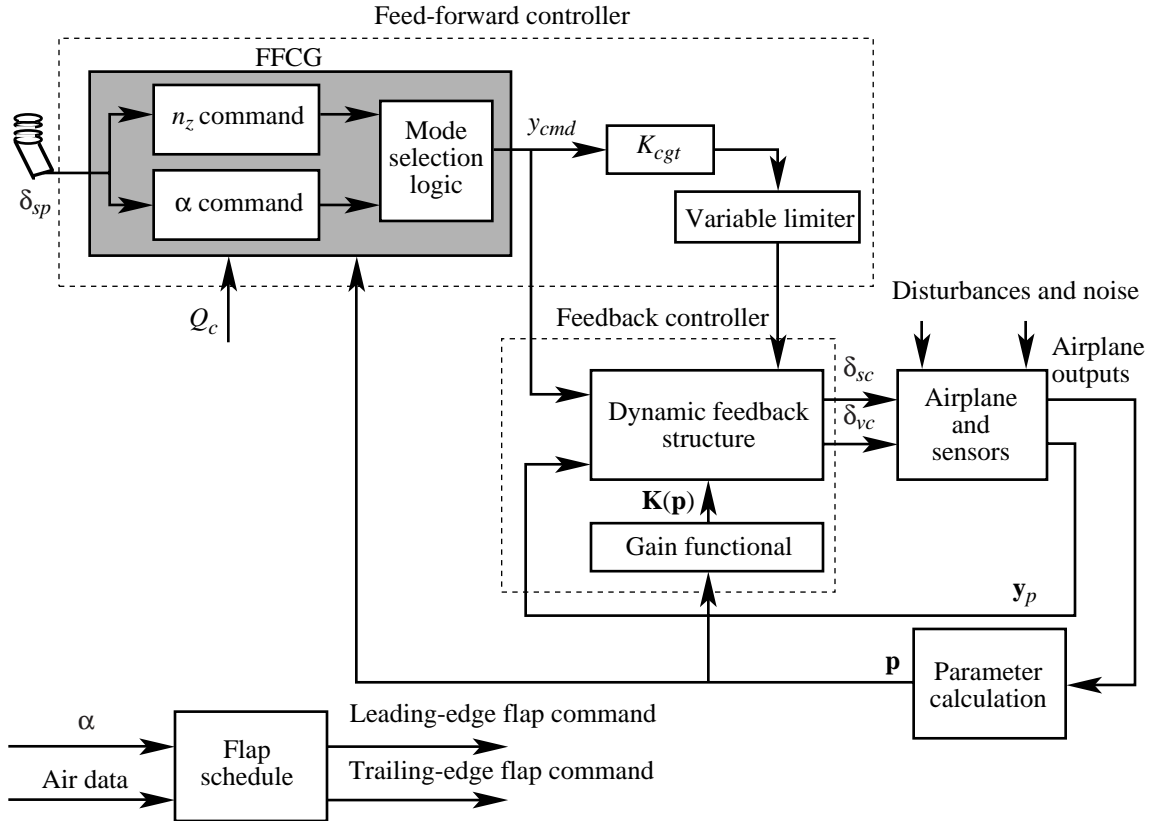


Figure 2. Block diagram of HARV longitudinal controller.

structure and gain functional. The gain functional generates feedback gain matrices  $\mathbf{K}(\mathbf{p})$  as a function of parameter vector  $\mathbf{p}$ . Control signals for the symmetric stabilator command  $\delta_{sc}$  and the pitch thrust-vectoring command  $\delta_{vc}$  are input to the airplane and generate airplane responses as measured by the sensors. Measured signals  $\mathbf{y}_p$  are fed back to the feedback controller while other measurements are used to calculate  $\mathbf{p}$  for both the feedback gain functional and the FFCG. The  $\mathbf{p}$  used for the FFCG contains one of the measurements used for the feedback controller. An additional part of the controller is the flap scheduler, which generates commands for both the leading- and trailing-edge flaps as a function of  $\alpha$  and air data measurements. The flap schedule is the same as used on the production F/A-18.

**Feed-forward controller.** The feed-forward controller converts pilot input commands to feedback controller commands by using the appropriate mode. A detailed description and derivation of the feed-forward control equations are presented in reference 2, and a summary of changes made for the CY 1994 flights is given in reference 3. A block diagram of the baseline flight FFCG is shown in figure 3 in which two solutions are continually generated. One solution is based upon the  $n_{z,c}$  mode by using a steady-state stick sensitivity of 1.0 g/in., while the other solution is based upon the  $\alpha_c$  mode by using a steady-state stick sensitivity of 10°/in. Gains  $K_{F1}$  and  $K_{F2}$  vary with flight conditions that are defined by elements within  $\mathbf{p}$ ; these gains are calculated by using functional relationships generated off-line by a least squares solution (ref. 2). The solution selected is the smallest absolute value comparing signals  $y_{1c}$  and  $y_{2c}$ . A trim bias  $\alpha_{oc}$  is added to the selected feed-forward stick gain signal to form the total feed-forward command  $y_{cmd}$ . This bias is 20° in the  $\alpha_c$  mode and was selected to yield a maximum command of  $\alpha = 70^\circ$  with 5 in. of pitch stick. Two nonlinear equations are used to generate the trim bias. One equation is for a 1g trim solution that is a function of impact pressure  $Q_c$ , and the other is an incremental term that is a function of  $Q_c$  and  $n_{z,c}$  (ref. 3). Under 1g flight, the trim bias allows the pilot stick to remain near the neutral position up to  $\alpha = 20^\circ$ .

The output of the FFCG is input both to the feedback controller and to the feed-forward gain  $K_{cgt}$  (fig. 2), which is fixed at  $-40$ . The output signal from  $K_{cgt}$  goes to a variable limiter where the limits change with flight conditions to maximize agility by allowing the controls to just reach saturation with maximum  $\delta_{sp}$  commands. The variable command limits were tuned for the various flight conditions by trial and error, with the values remaining within the lower and upper bounds set at 10 and 60, respectively.

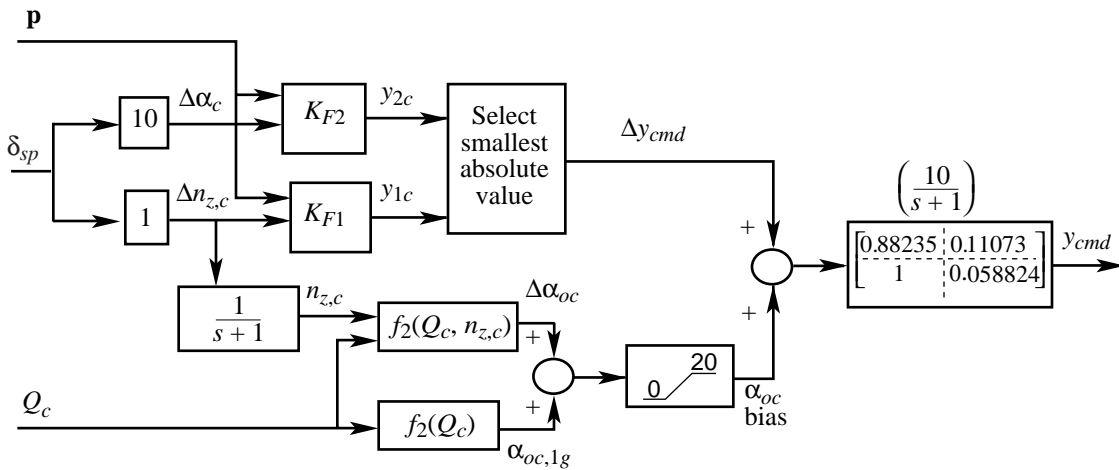


Figure 3. Block diagram of FFCG.

**Feedback controller.** The feedback controller is a rate-command system with a proportional-integral structure and a filter loop (PIF) and is implemented incrementally (refs. 8 and 9) as shown in figure 4. In this implementation, the proportional feedback-gain matrix  $\mathbf{K}_y(\mathbf{p})$  multiplies the incremental change in feedback vector  $\mathbf{y}_p$ ; the integrator feedback gain  $K_z(\mathbf{p})$  multiplies the difference between the sum of the measured feedback signals and the command, and the control filter feedback gain  $K_u(\mathbf{p})$  is incorporated into the discrete filter loop. Three elements of  $\mathbf{y}_p$  are angle of attack  $\alpha$ , pitch rate  $q$ , and load factor  $n_z$ ; thus, matrix  $\mathbf{K}_y(\mathbf{p})$  is composed of three scalar gains  $K_\alpha(\mathbf{p})$ ,  $K_q(\mathbf{p})$ , and  $K_n(\mathbf{p})$ . Matrix  $\mathbf{H}_{zy}$  is a row vector of three ones that allows summation of the three feedback signals to the integrator path. The rate command  $v_c$  is then passed through an integrator to generate the position command  $y_u$ , which is then separated into two signals for the stabilator command  $\delta_{sc}$  and the pitch thrust-vectoring command  $\delta_{vc}$ . Position limiters are incorporated to prevent windup in the rate-to-position integrator. The discrete dynamics in the  $\delta_{vc}$  actuator loop represent the Tustin transformation for a low-pass filter with a bandwidth of 1 rad/sec and a sampling period of 0.0125 sec. The implementation from  $y_u$  to  $\delta_{vc}$  represents a limited washout filter.

One advantage of the incremental approach is that sensor biases are subtracted out in the proportional feedback path. In the integrator path, the pilot can move the pitch stick slightly to compensate for biases. During trim, the error  $\Delta y$  in the integrator path is nulled by adjusting the stick input. As shown in figure 4, the feed-forward input signal to gain block  $K_{cgt}$  is also implemented incrementally.

### Modified Controller

The objective for the controller modifications was to trade off some agility in order to achieve satisfactory fine-tracking characteristics. An attempt was made to meet this objective with few changes to

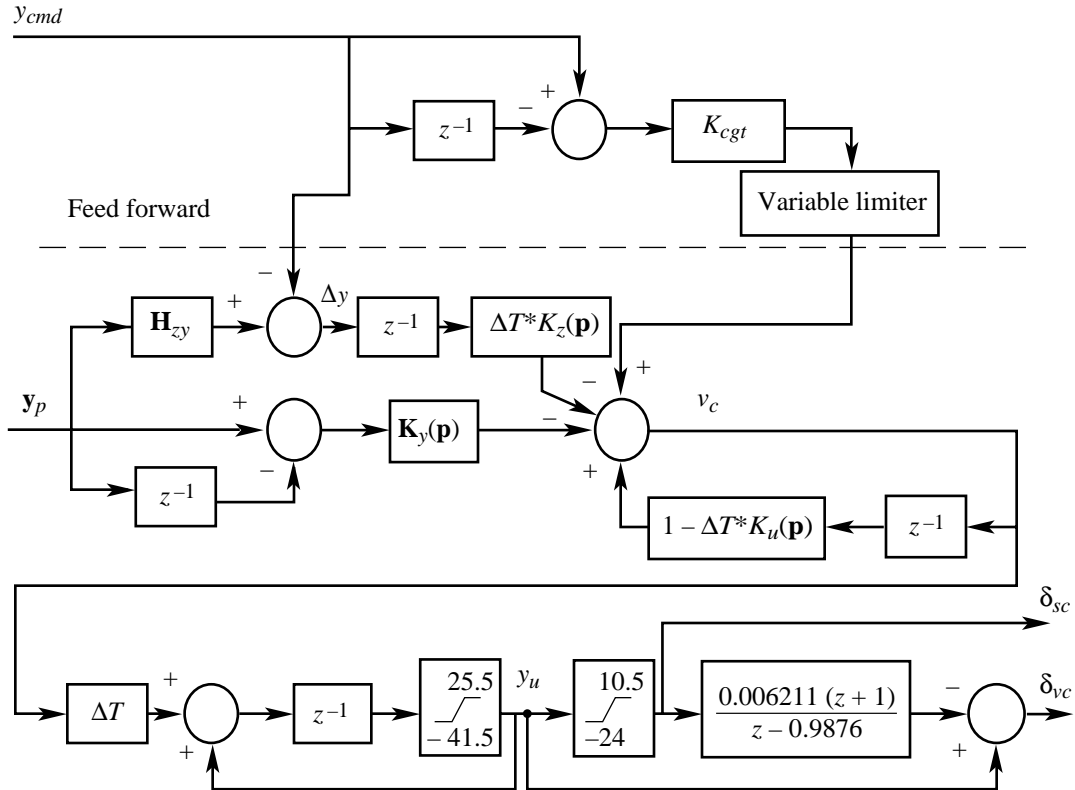


Figure 4. Feedback controller implementation for HARV with connection to feed-forward controller.

the feedback controller because the design had very good stability margins over the entire flight regime and also was highly robust to variations in stability and control derivatives. Therefore, it was decided to concentrate on the feed-forward controller, which was completely modified and simplified, as shown in figure 5.

Design objectives included reduced gains relative to the baseline controller, constant gains if possible, and simplification. The constant gains contrast with the baseline controller that allowed the gains to continuously vary with flight condition. In the modified controller, a constant gain of 10 is used for the feed-forward stick gain  $K_{ff}$ . This value for  $K_{ff}$  was chosen to allow  $y_{cmd}$  to reach  $70^\circ$  when the trim bias is  $20^\circ$ .

One problem created by the reduced value of  $K_{ff}$  was a loss of agility in reaching high angle of attack from high-speed (i.e., Mach 0.6), low angle-of-attack flight. The reason for this loss of agility is that the initial trim bias  $\alpha_{oc}$  is low, and the instantaneous value for  $y_{cmd}$  is below  $60^\circ$ , thereby reducing the overall nose-up command. Agility was recovered by adding a stick gain boost that increased the feed-forward gain from 10 up to a maximum of 14, depending upon  $Q_c$  and  $\delta_{sp}$ . This boost only comes into play when  $\delta_{sp} > 4$  in. and when  $Q_c > 61$  lb/in<sup>2</sup>. Maximum gain is achieved when  $\delta_{sp}$  is 5 in. and when  $Q_c > 150$  lb/in<sup>2</sup>.

Another major change was the calculation of the trim bias  $\alpha_{oc}$ . The block labeled “Original trim equation” in figure 5 is the same 1g trim equation used in the baseline controller. However, because the slope of the original trim equation becomes steep as  $Q_c$  decreases, it is now only used when  $Q_c \geq 120$  lb/in<sup>2</sup> to reduce sensitivity. The second trim equation is linear and is selected when  $Q_c$  is below 120 lb/in<sup>2</sup>, resulting in a sensitivity reduction of approximately 2.5. The upper trim bias limits were extended to  $23^\circ$  to help relieve stick forces caused by the lower feed-forward gain.

The feed-forward gain  $K_{cgt}$  has been reduced in magnitude from  $-40$  to  $-20$ , and the variable limiter shown in figure 2 has been removed. This new gain has been chosen based upon Neal-Smith (ref. 10) linear analysis made at various flight conditions. The two signals ( $y_{cmd}$  and the output from the  $K_{cgt}$  block) going to the feedback controller are identical to the baseline version except that  $y_{cmd}$  is not output from a low-pass filter in the modified controller.

Subsequent piloted ground-based simulation showed that the control system was still sensitive after making the feed-forward controller modifications; therefore, after some additional analysis, a decision was made to reduce the integrator gain in the proportional-integral portion of the feedback controller.

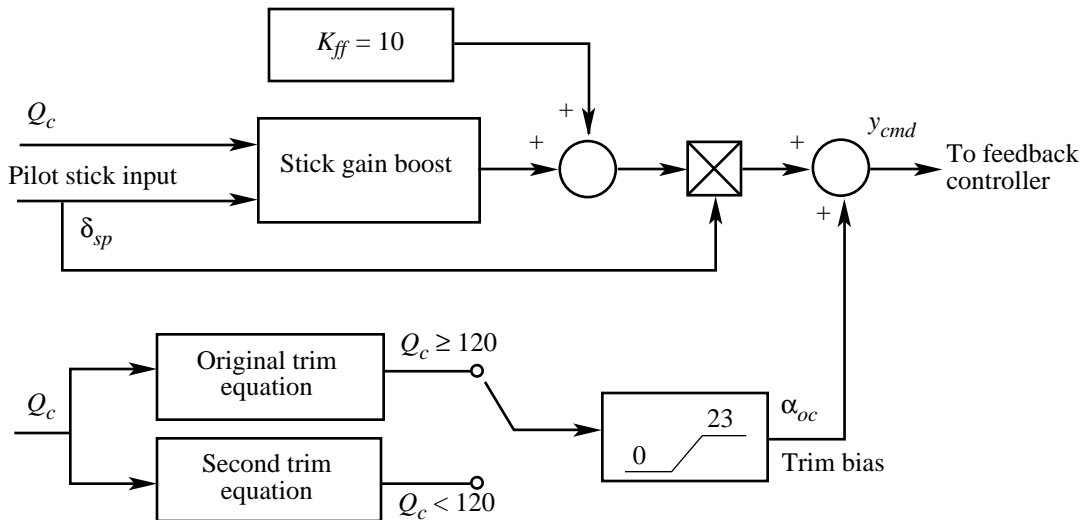


Figure 5. Block diagram for modified feed-forward controller.

For the Variable-Gain control methodology, it is impossible to change one gain without causing some change in other gains. However, the dominant change was reduction of the integrator gain in the  $\alpha = 20^\circ$  to  $\alpha = 50^\circ$  region where sensitivity was observed. The gain change for several design models was accomplished by increasing the integrator output noise intensity. (See table IV in ref. 3.) The control design algorithm is stochastic, and the gain in a sensor channel will normally decrease when the measurement noise for that sensor is increased. The Neal-Smith analysis was used to evaluate the modified gains for satisfactory fine target tracking. A discussion of the Neal-Smith analysis is presented in the “Linear Analysis” section of this paper.

Based upon the CY 1994 flight results, there was lack of confidence in the ground-based simulator for determining PIO during fine tracking, and a decision was made to evaluate three gain sets during actual flight. The pilot would be able to select these gain sets by using a switch in the cockpit. The feedback controller structure is identical to that shown in figure 4 except for the different gain sets. Two reduced gain sets were designed, giving three gain sets for flight evaluation; these gain sets are defined as low gain, medium gain, and high gain. The high-gain set is identical to the gains used in the baseline controller. The dominant change in the other two gain sets is a reduction in  $K_z(\mathbf{p})$  in the region between  $\alpha = 20^\circ$  and  $\alpha = 50^\circ$ . Specifically, the medium-gain set reduced the integrator gain by approximately a factor of 2 at  $\alpha = 35^\circ$ , and the low-gain set reduced the original integrator gain by a factor of 4 at the same flight condition. Smaller gain reductions occurred at the other flight conditions. The proportional feedback gain  $K_\alpha(\mathbf{p})$  changed along with the integrator gain. This gain increased by approximately a factor of 1.4 in the medium-gain set and by a factor of 2 in the low-gain set. In both the low- and medium-gain sets,  $K_n(\mathbf{p})$  has been set to zero because load factor is negligible at high  $\alpha$ , and it is a noisy signal that is a source of sensitivity.

Table 1 shows the trims for the 13 design cases used at an altitude of 25000 ft (design cases 15 to 27 from ref. 3), with the first 6 design cases (15 to 20) being trimmed for 1g unaccelerated flight. Figure 6 shows plots of the gains as a function of model number for these 1g trim design conditions. The gains are not plotted as a function of one parameter such as  $\alpha$  because speed is the dominant parameter for design cases 15 and 16. The variable-gain components used to calculate these gains and the modified stochastic weights used in the design algorithm are given in the appendix.

## Linear Models

This section describes the linear models used for feedback controller analysis and for flying qualities analysis of the entire control system. The first subsection describes the feedback controller, and the last subsection describes the feed-forward controller.

Table 1. Design Conditions at Altitude of 25000 Ft

Design case	Mach number	$\alpha$ , deg	Normal load factor, g units
15	0.70	3.58	1.00
16	.59	5	1.0
17	.33	20	.94
18	.26	35	.88
19	.26	50	.89
20	.28	65	.92
21	.70	20	4.2
22	.60	20	3.2
23	.60	35	4.5
24	.40	20	1.4
25	.40	35	2.0
26	.30	5	.24
27	.10	45	.14

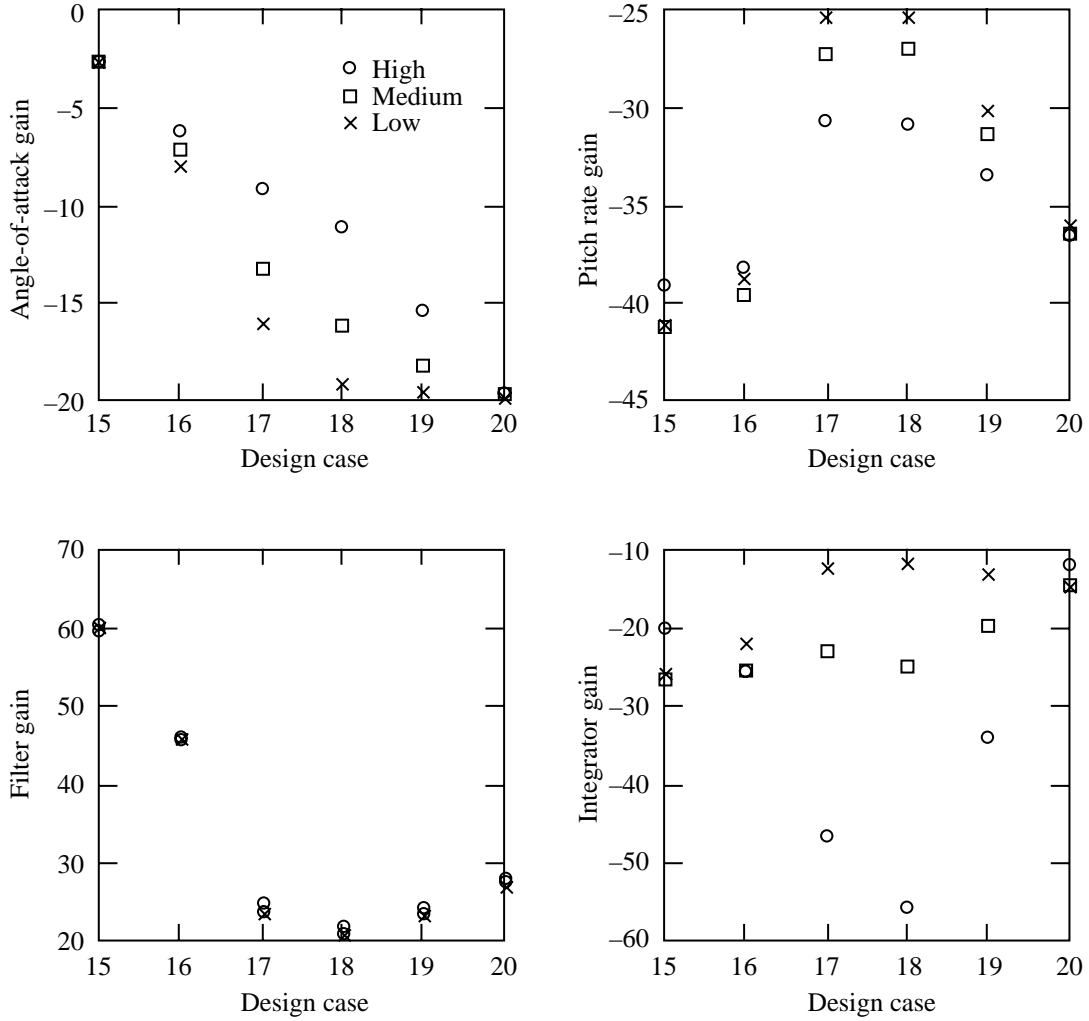


Figure 6. Comparison of feedback controller gains.

### Feedback Controller

Figure 7 is a linear representation for the feedback controller with variables for the inputs, output, and states. The command output  $y_u$  is shown prior to the split signal between the symmetric stabilator and pitch thrust-vectoring commands. Depending on the type of analysis performed, the Tustin transformation for the thrust-vectoring washout filter is either added to the controller output or inserted at the input to the airplane model.

The discrete dynamic equations that describe the feedback controller are shown below as

$$x_{c1,k+1} = \mathbf{H}_{zy} \mathbf{y}_{p,k} - y_{m1,k} \quad (1)$$

$$\mathbf{x}_{c2,k+1} = \mathbf{y}_{p,k} \quad (2)$$

$$x_{c3,k+1} = -\Delta T K_z(\mathbf{p}) x_{c1,k} + \mathbf{K}_y(\mathbf{p}) \mathbf{x}_{c2,k} + [1 - \Delta T K_u(\mathbf{p})] x_{c3,k} - \mathbf{K}_y(\mathbf{p}) \mathbf{y}_{p,k} + y_{m2,k} \quad (3)$$

$$x_{c4,k+1} = \Delta T x_{c3,k+1} + x_{c4,k} \quad (4)$$

$$y_{u,k} = x_{c4,k} \quad (5)$$

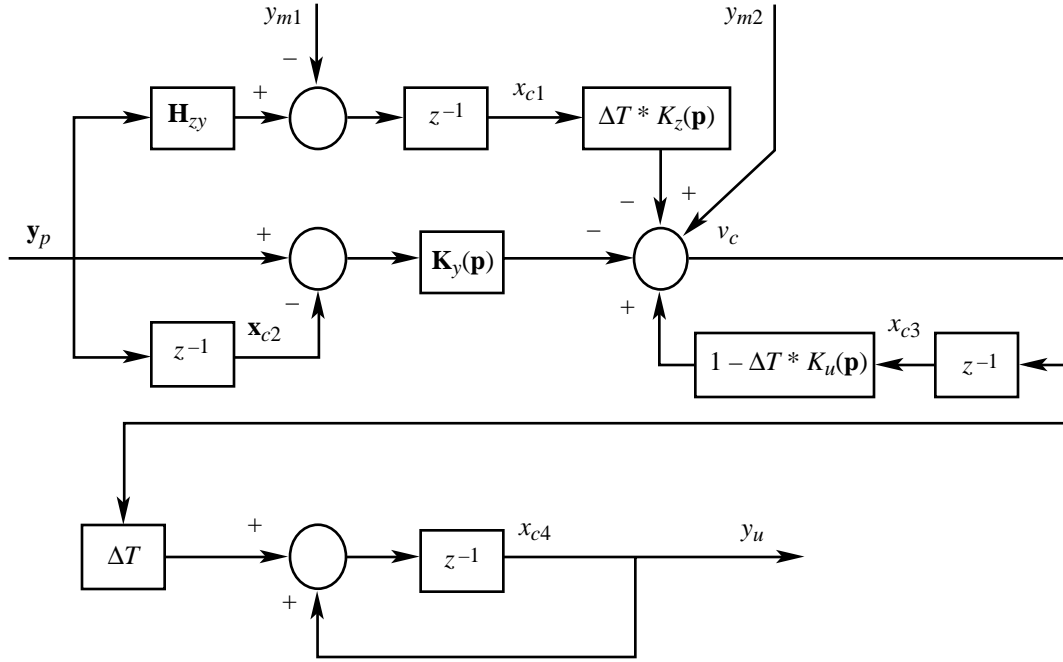


Figure 7. Linear model representation for feedback controller.

where  $k$  represents the present sample time and boldface symbols represent vectors or matrices. Equations (1) to (5) are combined to form the state space matrix equation for the feedback controller as

$$\begin{Bmatrix} x_{c1} \\ \mathbf{x}_{c2} \\ x_{c3} \\ x_{c4} \end{Bmatrix}_{k+1} = \begin{bmatrix} 0 & 0 & 0 & 0 \\ 0 & 0 & 0 & 0 \\ -\Delta T K_z(\mathbf{p}) & \mathbf{K}_y(\mathbf{p}) & 1 - \Delta T K_u(\mathbf{p}) & 0 \\ -\Delta T^2 K_z(\mathbf{p}) & \Delta T \mathbf{K}_y(\mathbf{p}) & \Delta T [1 - \Delta T K_u(\mathbf{p})] & 1 \end{bmatrix} \begin{Bmatrix} x_{c1} \\ \mathbf{x}_{c2} \\ x_{c3} \\ x_{c4} \end{Bmatrix}_k + \begin{bmatrix} \mathbf{H}_{zy} & -1 & 0 \\ \mathbf{I} & 0 & 0 \\ -\mathbf{K}_y(\mathbf{p}) & 0 & 1 \\ -\Delta T \mathbf{K}_y(\mathbf{p}) & 0 & \Delta T \end{bmatrix} \begin{Bmatrix} \mathbf{y}_p \\ y_{m1} \\ y_{m2} \end{Bmatrix}_k \quad (6)$$

$$y_{u,k} = [0 \ 0 \ 0 \ 1] \begin{Bmatrix} x_{c1} \\ \mathbf{x}_{c2} \\ x_{c3} \\ x_{c4} \end{Bmatrix}_k \quad (7)$$

## Feed-Forward Controllers

**Modified controller.** Referring to figure 8, a linear representation for the modified feed-forward controller is given as

$$x_{m1,k+1} = 0x_{m1,k} + K_{ff}\delta_{sp,k} \quad (8)$$

$$\begin{Bmatrix} y_{m1} \\ y_{m2} \end{Bmatrix}_k = \begin{bmatrix} 0 \\ -K_{cgt} \end{bmatrix} x_{m1,k} + \begin{bmatrix} K_{ff} \\ K_{cgt}K_{ff} \end{bmatrix} \delta_{sp,k} \quad (9)$$

where the outputs of this feed-forward model are inputs to equation (6). The feed-forward gains  $K_{ff}$  and  $K_{cgt}$  are constant over the entire flight regime for this controller.

**Baseline controller.** The linear model (shown in fig. 9) for the baseline feed-forward controller is more complicated than that for the modified controller because of nonlinearities and special conditions. The top section is used only for high-speed cases when the trim bias  $\alpha_{oc}$  is below  $20^\circ$ . Tustin transformations are used for each of the first order filters, which are also shown in continuous form. A nominal value of  $-40$  is used for gain  $K_{cgt}$ , although the variable limiter shown in figure 4 could result in reductions of this gain if the limits are reached. A describing function could be used to evaluate the effect of saturation.

The trim bias  $K_{tr}$  is a nonlinear function of  $\eta_{zc}$  (which is a function of the stick position) for a given value of  $Q_c$  with a form (ref. 3) shown as

$$y = a_0u + a_1u^2 + a_2u^3 + a_3u^4 \quad (10)$$

where

$$u = \frac{100\eta_{zc}}{Q_c} \quad (11)$$

Differentiating both sides of equation (10) gives

$$dy = a_0 du + 2a_1u du + 3a_2u^2 + 4a_3u^3 du|_{u=u_0} \quad (12)$$

where the control  $u$  is evaluated at some trim condition  $u_0$ . For high-speed cases, the pitch stick is usually in the vicinity of zero; therefore,  $u_0$  is assumed to be 0. Using a first order approximation for the linear analysis gain gives a value of  $K_{tr} = 6.9$ .

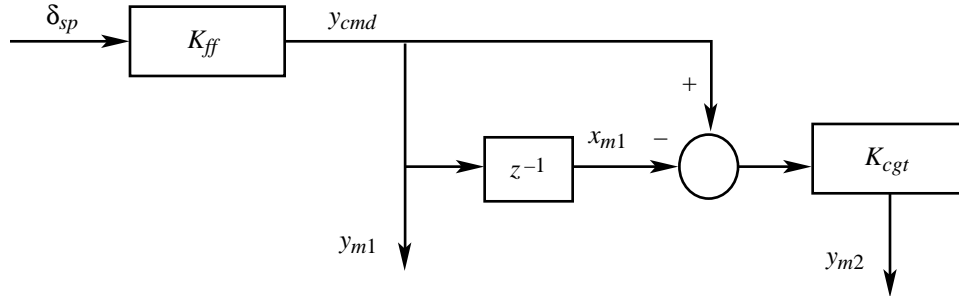


Figure 8. Linear model representation for modified feed-forward controller.

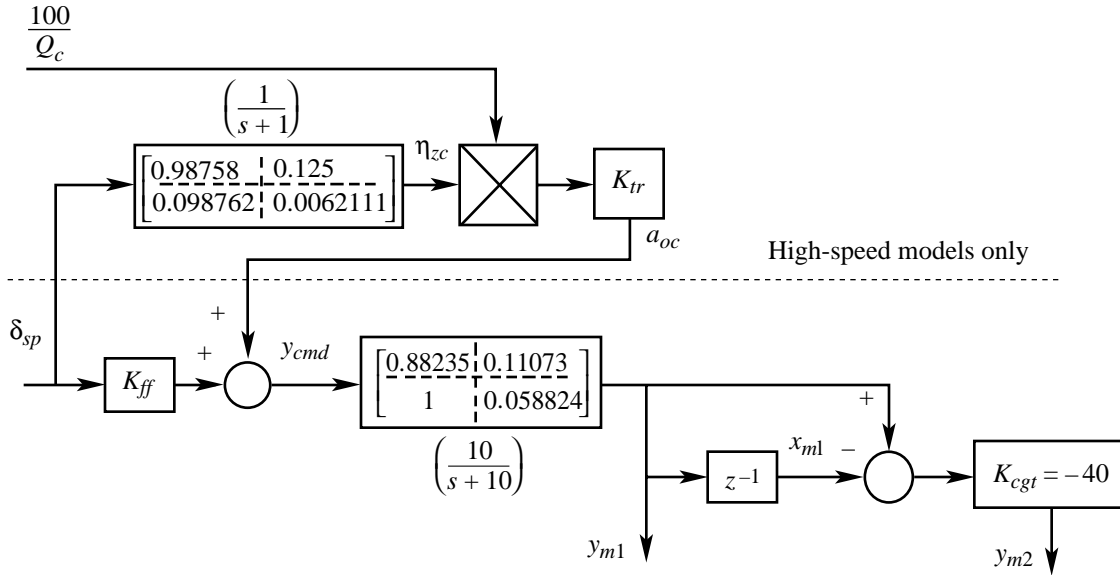


Figure 9. Linear model representation for baseline feed-forward controller.

### Closed-Loop Feedback Model

The linear feedback and feed-forward controllers have been combined with a washout filter for the pitch thrust-vectoring control and the airplane model with actuators and sensors to form the configuration shown in figure 10. The closed-loop feedback model consists of the feedback controller, washout filter, and airplane model. Different types of analysis such as single-loop Bode analysis, loop transfer analysis, and robustness analysis can then be made by breaking the feedback loop at selected locations. The transfer function from pilot stick input to any output can be evaluated by combining the feed-forward controller with the closed-loop feedback model. This configuration allows evaluation of flying qualities. One type of flying qualities evaluation is the Neal-Smith analysis (ref. 10), in which the typical transfer function from  $\delta_{sp}$  to pitch attitude  $\theta$  is used. Another flying qualities evaluation is the recently developed Bode envelope criteria (ref. 11), in which the output  $\alpha$  is used. The next section will show results of these different analyses.

### Linear Analysis

This section includes results of the linear analysis made for the three gain sets of the modified controller. The first three subsections apply only to the feedback controller. For these cases, results for the high-gain set also apply to the baseline feedback controller and have been documented in reference 3. The last two subsections include flying qualities analyses, which are only shown for the modified controller.

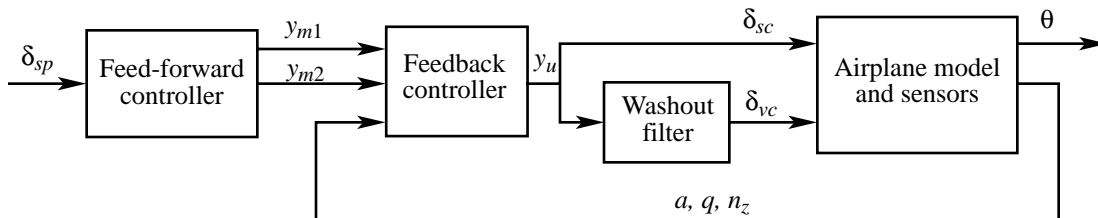


Figure 10. Feed-forward and closed-loop feedback models.

## Single-Loop Bode Analysis

Bode gain and phase margins were analyzed by using the linear feedback controller model (eq. (6)) with the addition of structural filters at the  $q$  and  $n_z$  sensor inputs. The feedback controller was connected to a high-order plant that included actuator dynamics, sensor dynamics, and antialiasing filters (ref. 3). The washout filter (fig. 4) was included as part of the plant, and the input to the plant was considered to be at test point  $y_u$  where the loop was broken. Table 2 contains the margins at the plant input for all three gain sets for design case models 15 through 27 (see table 1 for design conditions). The high-gain set has slightly lower margins compared to the data shown in reference 3 because this analysis includes the structural filters. The largest difference is  $5^\circ$  for the high-speed cases in which crossover frequencies are approximately twice those of the low-speed high-alpha cases; the structural filter dynamics would have a larger effect on these high-speed cases.

Table 2. Bode Margins at Plant Input for Three Gain Sets

Design case model	High-gain set		Medium-gain set		Low-gain set	
	Gain margin, dB	Phase margin, deg	Gain margin, dB	Phase margin, deg	Gain margin, dB	Phase margin, deg
15	7.5	52.9	7.5	53.3	7.5	53.4
16	7.8	51.7	7.9	53.1	8.0	53.9
17	12.0	50.4	12.3	58.1	12.9	62.0
18	12.4	49.0	14.0	59.2	14.7	65.4
19	-25.2	53.9	-24.7	58.9	-25.2	61.1
	12.5		13.8		14.0	
20	23.1	61.5	19.7	61.5	19.6	61.1
21	7.6	53.5	7.8	54.3	7.7	54.5
22	7.7	51.9	8.0	53.8	8.0	54.6
23	8.4	53.9	8.5	56.5	8.5	57.5
24	10.2	51.4	11.4	58.2	11.8	61.3
25	10.4	51.7	11.5	59.7	11.9	63.5
26	11.2	50.9	12.9	58.5	13.7	61.7
27	16.2	52.6	17.7	63.2	18.2	69.3

All design case models meet the specifications of 6-dB gain margin and  $45^\circ$  phase margin. In the  $\alpha = 20^\circ$  to  $50^\circ$  range (models 17 through 19, 21 through 25, and 27), gain and phase margins generally increased with reduced integrator gain. The most critical loop at the plant output is the pitch rate output, and results for breaking that loop are very similar to those shown in table 2.

## Loop Transfer

In the next four subsections, *model* will be the shorthand notation for the design case model number. Figure 11 shows the loop transfer for the three gain sets for models 15 and 18 with the loop broken at the plant input. Loop transfer is a singular value analysis with all loops opened simultaneously. The maximum singular value gives an upper bound on the bandwidth. For the case of one loop, the response is the same as the Bode response.

Model 15 (high speed) has crossover frequencies between 7 and 8 rad/sec, while model 18 (the  $1g$   $\alpha = 35^\circ$  case) has crossover frequencies between 3 to 4 rad/sec. The low-gain set for model 18 shows a large-gain reduction at low frequency but only a small reduction in the crossover frequency. Model 15 shows little change with gain set. Crossover frequencies for the loop transfer at the plant output are very similar to those shown in figure 11.

## Structured Singular Value Analysis

A structured singular value analysis ( $\mu$  analysis) for a multiplicative error was evaluated at the plant output; this is a robustness analysis with all loops opened simultaneously. Figure 12 shows the complex  $\mu$  analysis results for the three gain sets for models 15, 17, 18, and 19. (See table 1.) Models 17 through

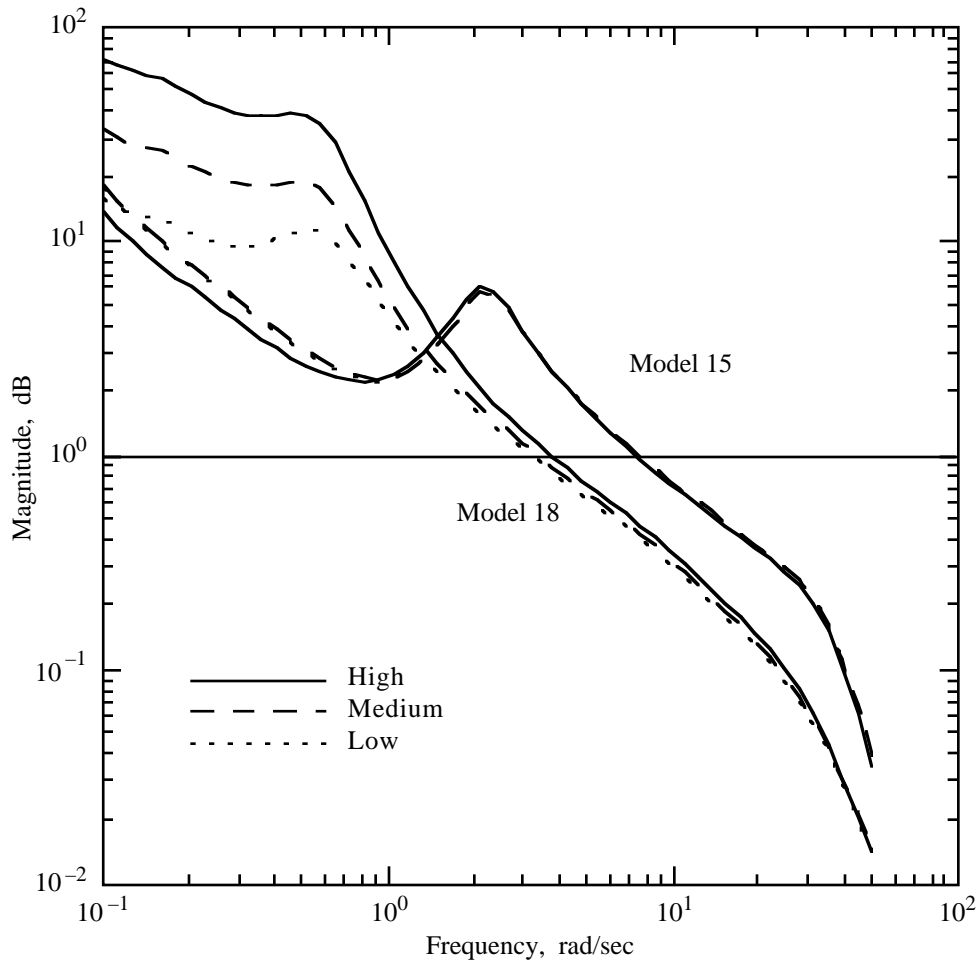


Figure 11. Loop transfer at plant input.

19 are in the  $\alpha$  range in which the redesigned gains were changed most (see fig. 6), with model 18 showing the largest variation with gain. The low-gain set is shown to have the greatest robustness with a minimum value of approximately 0.65 compared to 0.48 for the high-gain set. These minimums imply a range in which the gain and phase may simultaneously change without destabilizing the control system. For example, complex changes less than 65 percent in all outputs of the low-gain system can be tolerated without the system becoming unstable. In reference 3 a real  $\mu$  analysis showed much better results for the high-gain set for the condition where only real (not complex) variations are expected.

### Neal-Smith Analysis

Evaluation of flying qualities for the baseline controller was conducted by using fixed-base, real-time piloted simulation (refs. 3, 4, and 12). Analysis such as the Neal-Smith closed-loop criterion (ref. 10) was briefly investigated but was discounted because none of the research appeared applicable to high-alpha conditions. In fact, guidelines for high-alpha conditions were nonexistent. The Neal-Smith criterion was originally developed for highly augmented fighter aircraft performing precision tracking tasks, and it was decided to take a closer look at this criterion after experiencing flight tracking problems. Limited success with this criterion using high-alpha flight data was also reported by Keith D. Wichman.<sup>1</sup>

<sup>1</sup>Paper presented at the Fourth High-Alpha Conference, NASA Dryden Flight Research Center, July 12-14, 1994.

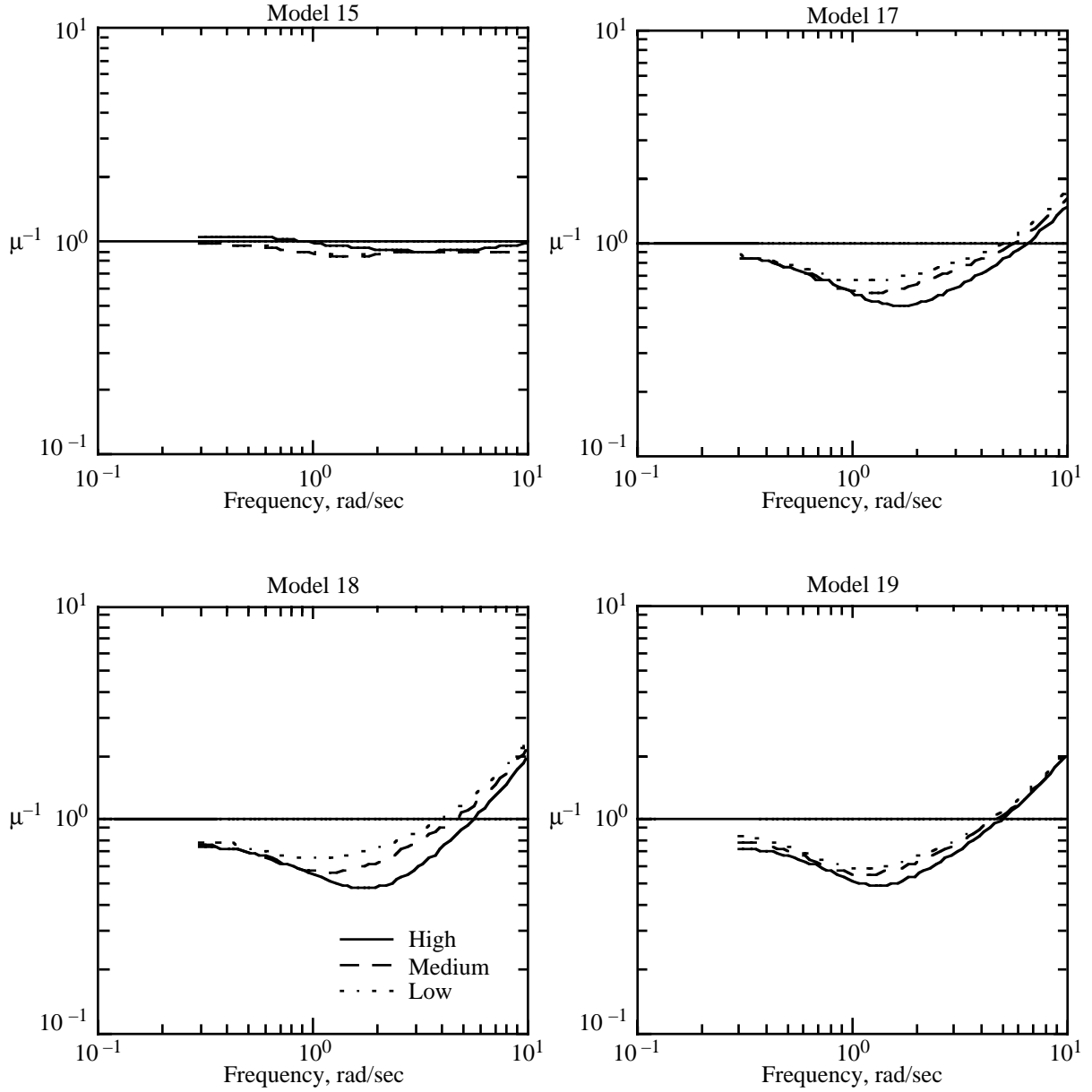


Figure 12. Results of  $\mu$  analysis at plant output.

The Neal-Smith criterion assumes a tracking task whereby the pilot operates only on pitch attitude tracking error ( $\theta_e$ ). The pilot model is composed of a pilot gain ( $K_p$ ), pilot time delay ( $\tau_p$ ), and a lead-lag transfer function with time constants ( $\tau_{LEAD}$ ) and ( $\tau_{LAG}$ ). The pilot model transfer function is shown below as

$$\frac{\delta_{sp}}{\theta_e} = K_p e^{-\tau_p s} \left( \frac{\tau_{LEAD} s + 1}{\tau_{LAG} s + 1} \right) \quad (13)$$

where the output of the pilot model is the pitch stick command, as shown in figure 13. The criterion assumes a certain degree of aggressiveness with which the pilot closes the loop and a desired level of performance. Aggressiveness is captured by the bandwidth frequency ( $\omega_B$ ), whereas the desired level of performance is defined by the admissible droop. As illustrated in figure 14, bandwidth is the frequency

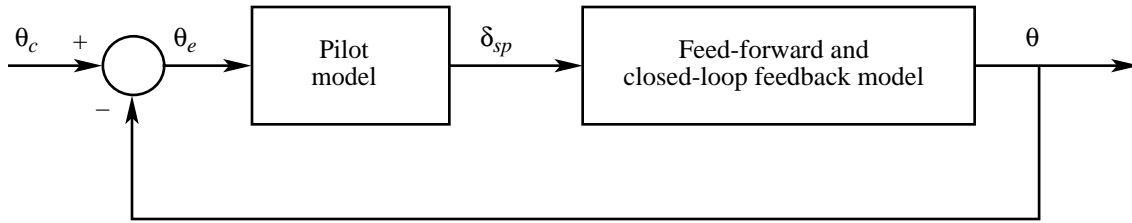


Figure 13. Configuration for Neal-Smith analysis.

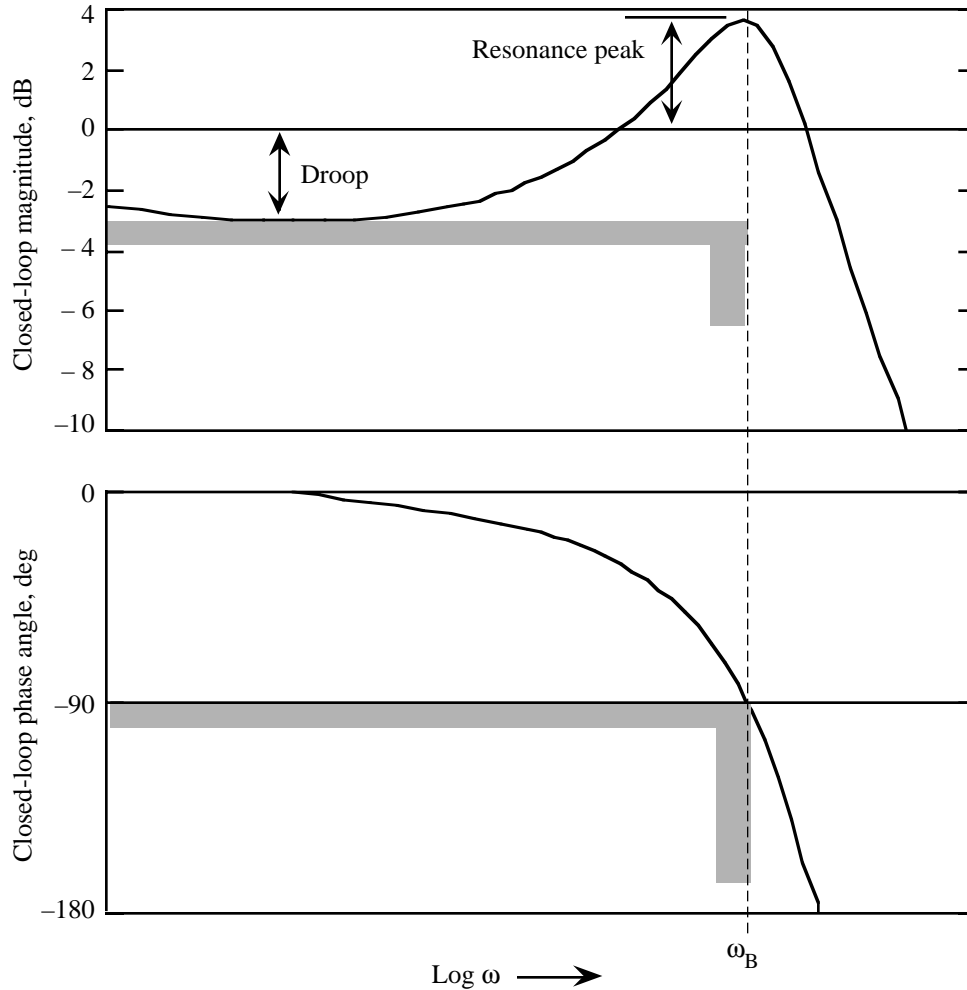


Figure 14. Neal-Smith criterion parameters.

at which the phase angle of the compensated closed-loop response is  $90^\circ$ , and droop is the minimum gain of the frequency response when the input frequency is below the specified  $\omega_B$  frequency. For a desired  $\omega_B$  and droop, the loop is closed and the various parameters are varied.

A computer program<sup>2</sup> was used to optimize the various parameters. The criterion output parameters are the pilot compensation required and the resulting oscillatory tendencies as measured by the closed-loop pitch attitude resonance. Pilot compensation is the phase angle of the pilot lead-lag compensator in

<sup>2</sup>Received from Dryden Flight Research Center and modified at Langley Research Center by Dr. Bart Bacon.

equation (13). Figure 15 illustrates the Neal-Smith parameter plane with typical pilot comments at different sections of the plane. The solid boundaries indicate pilot ratings (PR) that separate the three major Cooper-Harper Rating (CHR) levels (ref. 13); a CHR level 1 rating would be within the boundary  $PR = 3.5$ , a CHR level 2 rating would be between the boundaries labeled  $PR = 3.5$  and  $PR = 6.5$ , and a CHR level 3 rating would be greater than the  $PR = 6.5$  boundary.

In the computer program,  $\omega_B$  and  $\tau_p$  are specified along with the droop value. The pilot gain and the lead and lag time constants are adjusted within the computer program to optimize the closed-loop performance for the specified constraints. In the original analysis (ref. 10), a pilot time delay of 0.3 sec and a maximum droop of  $-3$  dB was imposed. An  $\omega_B = 3.5$  rad/sec was selected to be most representative of a fighter tracking and maneuvering environment. In reference 14, it is recommended that  $\omega_B$  be reduced to 3.0 rad/sec for the HARV airplane based upon engineering judgment and simulation results, implying that the task frequency requirements tend to decrease with increasing angle of attack. The HARV experience showed that the lower bandwidth was appropriate for correlation with flight results.

Figure 16 shows the Neal-Smith results for four models (15, 17, 18, and 19) and the three gain sets. For this analysis,  $\omega_B$  was varied from 2.5 rad/sec to 4 rad/sec in steps of 0.5 rad/sec, giving a total of four data points for each case. Straight lines were plotted between each data point as the frequency increased. The 4 rad/sec data point for model 18 with the high-gain set had a numerical problem, and thus was not plotted. The direction for the unplotted data point is illustrated by a wiggle sign in the figure. The  $\omega_B = 3$  rad/sec data point is shown for each gain set, with a solid square for low gain, a solid triangle for medium gain, and a solid circle for high gain.

Results show that the high-speed case (model 15) is generally within the level 1 boundary and that all three gain sets are approximately the same, as expected. The high-alpha cases (models 17 through 19) show that the high-gain set has a sensitivity problem and could have a tendency to PIO. For

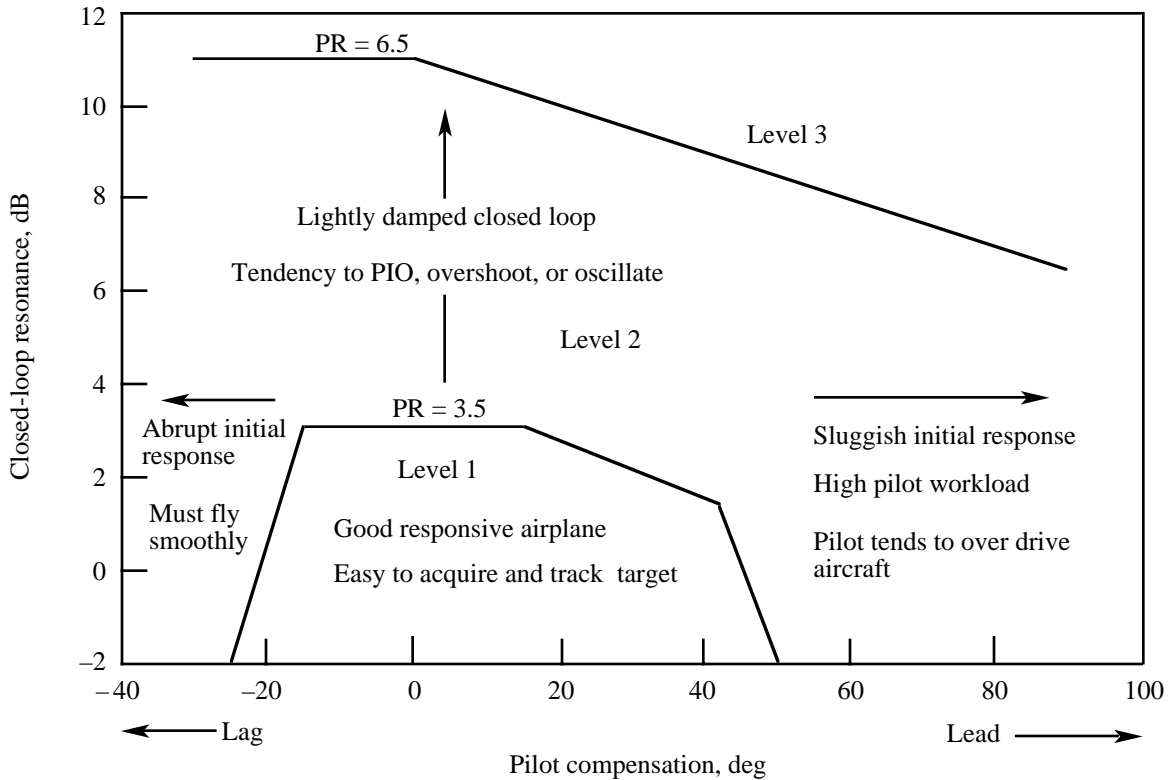


Figure 15. Neal-Smith parameter plane with typical pilot comments.

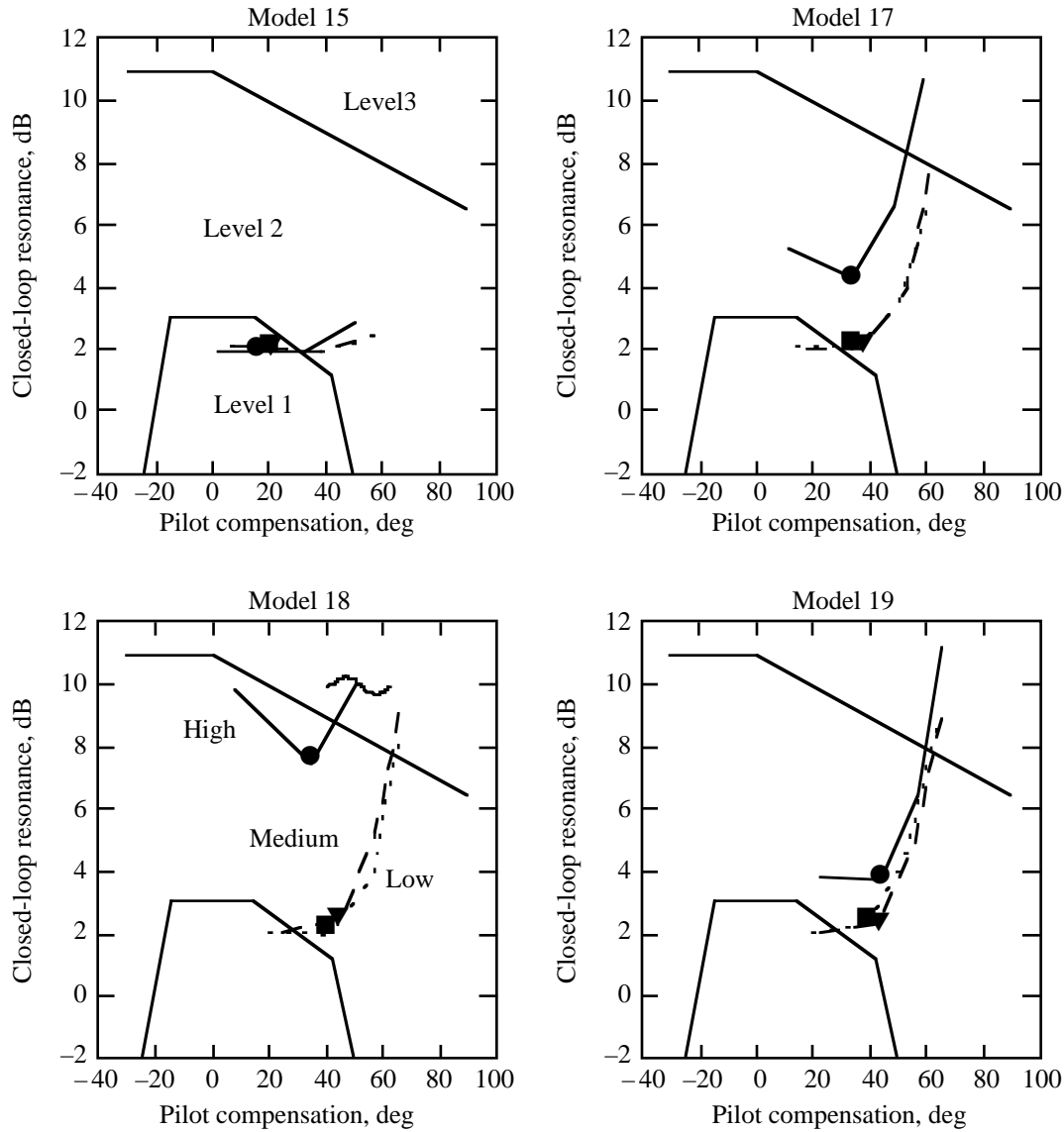


Figure 16. Results using Neal-Smith handling qualities analysis. Symbols represent the condition where  $\omega_B = 3$  rad/sec.

model 18 at  $\alpha = 35^\circ$  and  $\omega_B = 3.0$  rad/sec, the high-gain set has a closed-loop resonance close to the level 3 region. The low- and medium-gain sets for models 17 through 19 have significantly better results with the low-gain set being slightly better than the medium-gain set. At  $\omega_B = 3.0$  rad/sec, the performance is slightly beyond the level 1 boundary, and at  $\omega_B = 3.5$  rad/sec, the results are midway in the level 2 region.

### Bode Envelope Criteria

During the past several years, various flying qualities design guidelines have been investigated for application to high-alpha flight (ref. 11). A typical problem is that most criteria are expressed in terms of classical low-order system parameters that require identification of modes such as the short period and phugoid modes. Unfortunately, these modes are not always easily identifiable in closed-loop systems in which the control law has been designed using modern control design methodologies.

One analysis technique that appears promising and is easily usable for any design methodology is the high-alpha Bode envelope guidelines. Preliminary level 1 Bode guidelines have been developed for

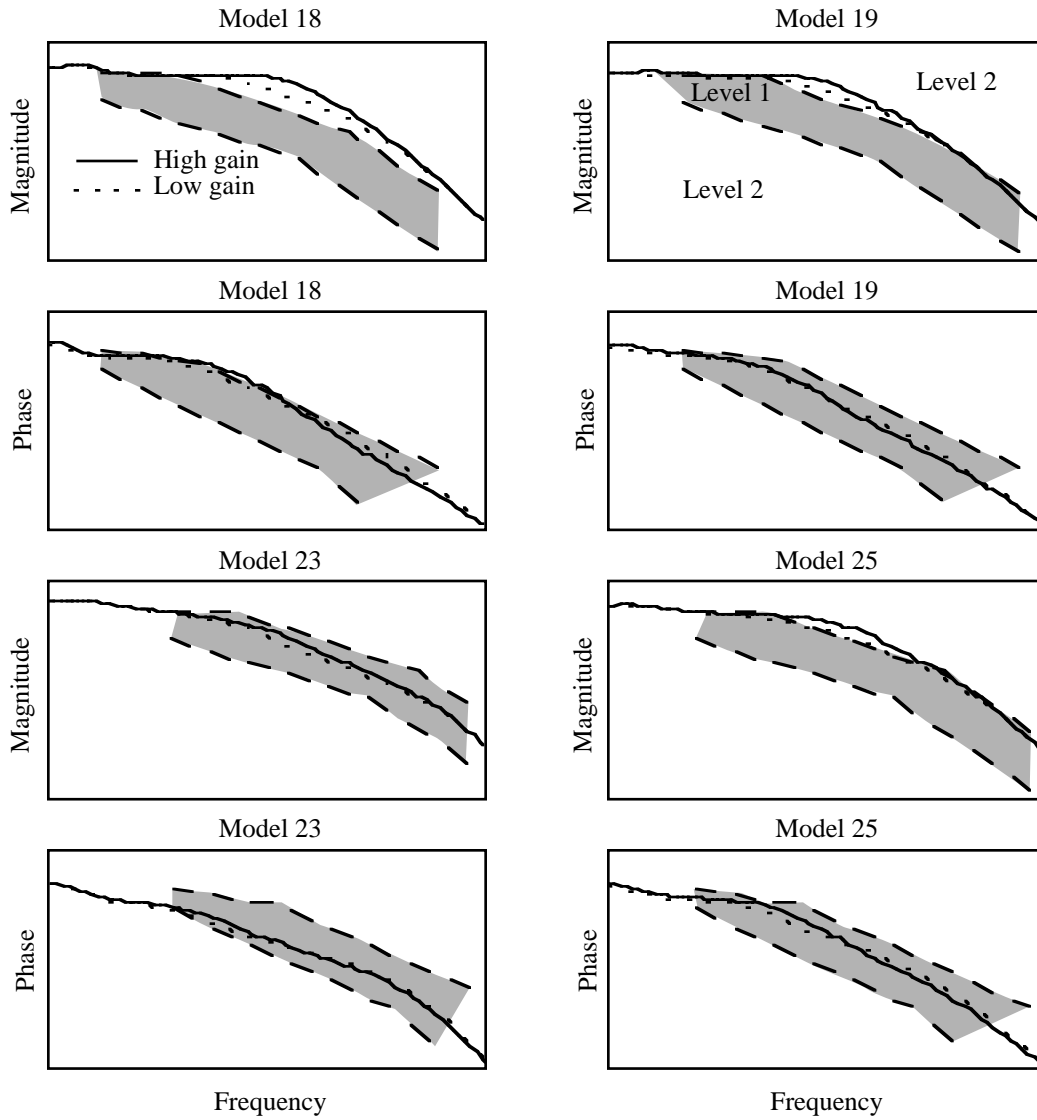


Figure 17. Bode envelope criteria and frequency response data for low- and high-gain sets. The shaded areas between the dashed lines are the envelope criteria specifying level 1 and level 2.

both tracking and acquisition at  $\alpha = 30^\circ$  and for post-stall flight. The discussion in this paper is for alpha-command systems, although the reference also includes guidelines for rate-command systems. The level 1 frequency boundaries (other levels have not been defined) of the alpha-command guidelines change with flight condition, and guidelines are different for tracking and acquisition. Because reference 11 contains restricted information, data values and tick marks are not included in this paper, and only a general discussion of results is provided. Publication of this reference was too late to use the Bode envelope guidelines during design, but they were used for postflight analysis.

Figure 17 contains the level 1 Bode envelope criteria and both low- and high-gain frequency response data for models 18, 19, 23, and 25 (see table 1). The frequency response data are from the configuration shown in figure 10, except that the output is  $\alpha$  rather than  $\theta$ . Trim conditions for models 18, 23, and 25 are all at  $\alpha = 35^\circ$  at load factors of 1g, 2g, and 4.5g, respectively. Data for these three cases are plotted for the  $\alpha = 30^\circ$  criterion. Model 19 has a trim of 1g at  $\alpha = 50^\circ$  and the data are plotted against the  $\alpha = 45^\circ$  criterion.

Results for this criterion indicate that magnitude is high for the low-speed 1g cases but improves as speed increases (higher load factor). Although the low-gain set magnitude for model 18 shows improvement, it is still slightly high, indicating that sensitivity could occur. Phase response appears to be good for all cases.

## Piloted Simulation

This section contains piloted simulation results performed at the Defence Research Agency (DRA) in Bedford, United Kingdom. The evaluations were conducted in the Large Motion System (LMS), which could be operated in either a fixed-base or in a motion-base mode. Objectives of the simulations were to evaluate the modified controller under motion with all three gain sets to determine whether motion has an effect in causing PIO with the baseline controller and to evaluate simulation realism relative to flight. The nonlinear dynamic model of the HARV was operational in this facility.

### Facility Description

The LMS provides motion in five axes: roll, pitch, yaw, heave, and either sway or surge. The choice between sway and surge is achieved by physically rotating the cockpit. All five axes are totally independent, and performance limits can be achieved simultaneously. Noteworthy features are large linear displacements with high velocities and accelerations, as shown in table 3 (ref. 15).

Table 3. Large Motion System Performance Limits

Motion	Maximum displacement	Maximum velocity	Maximum acceleration
Sway/surge.....	±13.1 ft	8.2 ft/sec	16.4 ft/sec <sup>2</sup>
Heave.....	±16.4 ft	9.8 ft/sec	32.8 ft/sec <sup>2</sup>
Roll.....	±0.5 rad	0.7 rad/sec	3.0 rad/sec <sup>2</sup>
Pitch.....	±0.5 rad	0.5 rad/sec	2.0 rad/sec <sup>2</sup>
Yaw.....	±0.5 rad	0.5 rad/sec	1.5 rad/sec <sup>2</sup>

Outside world visual cues are provided by a three-window computer-generated image (CGI) system. Each display monitor has a 48° horizontal by 36° vertical field of view, and the two outside monitors are rotated by 90° to give a total azimuth angle of 120°.

Cockpit orientation allowed the sway direction to move with the surge direction fixed, even though the longitudinal axis was being evaluated. One reason for selecting this orientation was to accommodate other programs that required the sway degree of freedom. Time requirements to reorient the cockpit are at least several hours, making it impossible to alternate from one program to another. Allowing sway to be free was considered more beneficial.

### Simulation Study

Four longitudinal-lateral target tracking tasks (two at high speed and two at high  $\alpha$ ) were used to evaluate the controllers. These tasks are defined as tasks A, B, C, and D for this paper and are summarized in table 4, along with the criteria for evaluation. The two high-speed tracking tasks are for moderate- $\alpha$ , elevated-g flight conditions (ref. 12), and track-a-target maneuvering at 3g. Task A has a nominal speed of Mach 0.6 (range from 0.55 to 0.65) with  $\alpha$  varying between 15° to 20°, whereas task B has a nominal speed of Mach 0.45 (range from 0.4 to 0.5) with  $\alpha$  varying between 20° and 25°. The two high-alpha target-tracking tasks are also described in reference 12 with details in references 16 and 17. Task C is an  $\alpha = 30^\circ$  target-tracking task, and task D is for  $\alpha = 45^\circ$ .

Table 4. Target-Tracking Tasks

Task	Maneuver
A	<p>Initial conditions: Mach = 0.6, altitude = 25000 ft, HARV 600 ft behind target, same heading and altitude.</p> <p>Procedure: Target rolls into a 3g turn and holds for 30 sec, reverses bank angle, and continues to reverse every 10 sec for end time of 60 sec.</p> <p>Criteria: Keep target within a 12.5-mrad-diameter reticule 50 percent of time for desirable criteria and 10 percent of time for adequate criteria.</p>
B	<p>Initial conditions: Mach = 0.45, altitude = 25000 ft, HARV 600 ft behind target, same heading and altitude.</p> <p>Procedure: Target rolls into a 3g turn and holds for 30 sec, reverses bank angle, and continues to reverse every 10 sec for end time of 60 sec.</p> <p>Criteria: Keep target within a 12.5-mrad-diameter reticule 50 percent of time for desirable criteria and 10 percent of time for adequate criteria.</p>
C	<p>Initial conditions: Mach = 0.5, altitude = 25000 ft, HARV 1500 ft behind target, same heading and altitude.</p> <p>Procedure: Target advances throttles to maximum, rolls the airplane into a turn, and maneuvers to <math>\alpha = 25^\circ</math>. HARV rolls behind the target by using military power, advances throttles to maximum, and pulls pitch stick back to track at <math>\alpha = 30^\circ</math>.</p> <p>Criteria: Keep target within 5 mrad of aim point 50 percent of time and within 25 mrad the rest of the time for desirable criteria. For adequate criteria keep target within 5 mrad of aim point 10 percent of time and within 25 mrad of aim point the rest of the time. No objectionable PIO should be observed.</p>
D	<p>Initial conditions: Mach = 0.5, altitude = 25000 ft, HARV 1500 ft behind target, same heading and altitude.</p> <p>Procedure: Target advances throttles to maximum, rolls the airplane into a turn, and maneuvers to <math>\alpha = 30^\circ</math>. HARV rolls behind the target by using military power, advances throttles to maximum, and pulls pitch stick back to track at <math>\alpha = 45^\circ</math>.</p> <p>Criteria: Keep target within 5 mrad of aim point 50 percent of time and within 25 mrad the rest of the time for desirable criteria. For adequate criteria keep target within 5 mrad of aim point 10 percent of time and within 25 mrad of aim point the rest of the time. No objectionable PIO should be observed.</p>

Each controller was evaluated separately by using a complete set of maneuvers. All tracking tasks were first evaluated by using a fixed-base configuration, and the tasks were repeated by using the motion-base configuration. This approach allowed direct comparison between fixed-base and motion-base results. The same lateral-directional controller was used for all maneuvers.

The sequence of events was to evaluate the baseline controller first because that was the only configuration flight-tested at the time of these simulations. Then the modified controller was evaluated, starting with the low-gain set, then the medium-gain set, and finally the high-gain set. As explained earlier in the section on controller description, the modified controller has the same feed-forward configuration for all three gain sets, and the high-gain set is the same as that used in the baseline flight controller. All evaluations were made by a NASA test pilot, who also flew the tracking tasks in the HARV during the baseline flight controller evaluations.

The pilot was instructed to give Cooper-Harper ratings (CHR) by using the rating scale shown in figure 18 (ref. 13), and pilot-induced oscillation (PIO) ratings (ref. 13) by using the rating scale shown in table 5. As shown in the table, PIO ratings are from 1 to 6, with 1 representing no tendency to induce undesirable motions and 6 representing a potential for divergent oscillations under normal control. Typically, a rating between 4 and 6 indicates PIO.

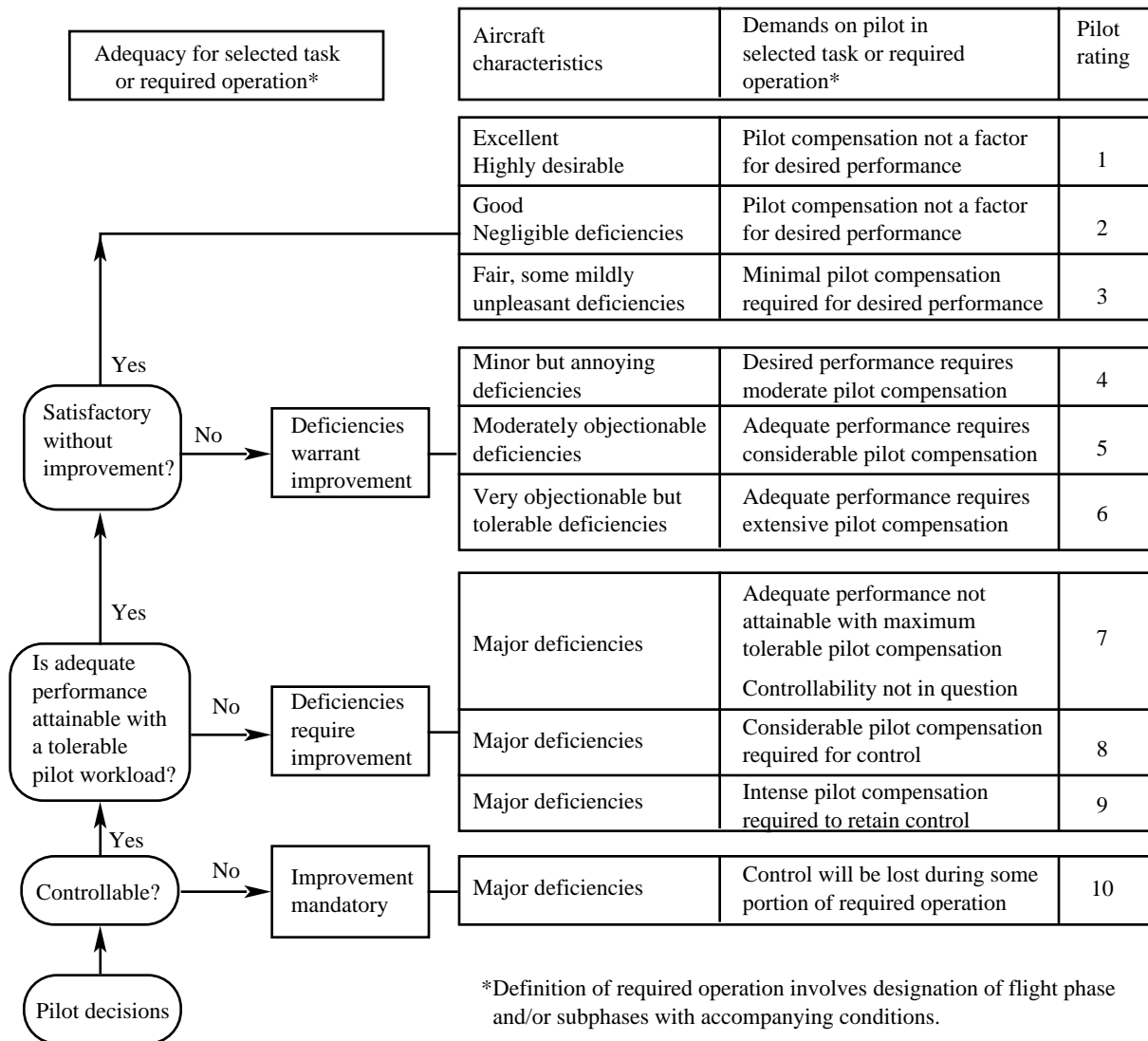


Figure 18. Cooper-Harper rating scale.

### Simulation Results

The CHR and PIO ratings (PIOR) for the different longitudinal controllers, both fixed base and motion base, are presented in table 6. In the table, “F” represents the fixed-base configuration and “M” represents the motion-base configuration.

Although all tracking tasks are for both longitudinal and lateral-directional tracking, the pilot was asked to give separate ratings for each axis. Only one run was made for all cases, except for maneuver C with motion, in which two runs were made by using the low-gain set. The reason for the repeated run is due to some unexpected residual oscillations of approximately 15 mrad, although generally desired performance was met. A second run showed no PIO tendencies and resulted in improved ratings.

The baseline controller was a good candidate to evaluate both the effect of motion in causing PIO and the realism of the motion-base simulation relative to flight because this controller exhibited PIO during flight tracking tasks B, C, and D (ref. 6). From the results and pilot comments, it is clear that the response of the motion-base simulation was only slightly more sensitive than the response of the fixed-base simulation. In this context, sensitivity refers to undesired motions of the airplane. Both

Table 5. Pilot-Induced Oscillation Rating Scale

Description	Rating
No tendency for pilot to induce undesirable motions.	1
Undesirable motions tend to occur when pilot initiates abrupt maneuvers or attempts tight control. These motions can be prevented or eliminated by pilot technique.	2
Undesirable motions easily induced when pilot initiates abrupt maneuvers or attempts tight control. These motions can be prevented or eliminated but only at sacrifice to task performance or through considerable pilot attention and effort.	3
Oscillations tend to develop when pilot initiates abrupt maneuvers or attempts tight control. Pilot must reduce gain or abandon task to recover.	4
Divergent oscillations tend to develop when pilot initiates abrupt maneuvers or attempts tight control. Pilot must fly open loop by releasing or freezing the stick.	5
Disturbance or normal pilot control may cause divergent oscillations. Pilot must open control loop by releasing or freezing the stick.	6

Table 6. Longitudinal CHR and PIOR Comparisons for Tracking Tasks With Fixed- (F) and Motion-Base (M) Simulation

Task	Type of rating	Baseline		Low gain		Medium gain		High gain	
		F	M	F	M	F	M	F	M
A	CHR	7	7	4	3	3	4	4	4
	PIOR	3	4	1	1	1	2	2	2
B	CHR	7	8	3	4	4	4	4.5	10
	PIOR	5	5.5	1	2	2	2	2.5	5
C	CHR	7	8	4	4.5/3	4	5	10	8
	PIOR	5	5	2.5	2.5/1	2	3	5	5
D	CHR	5	5.5	4.5	4	3	4.5	8	9
	PIOR	3	2.5	2	2.5	2	2	4.5	5

configurations exhibited PIO (ratings 4 through 6), with maneuvers B and C showing divergent oscillations. Under motion maneuver A also had oscillations whereas maneuver D only exhibited some undesirable motions. These results are contradictory to the baseline flight results because maneuver A is the only flight tracking task that did not have PIO. Different results might have been obtained if the motion-base simulator surge direction was allowed to be free with the sway direction fixed. Time did not allow the exploration of that configuration. Although the lateral-directional results are not discussed in this paper, the ratings were significantly worse than those obtained in flight. The pilot did comment that the motions felt more pronounced compared to flight. The benefit of motion-based simulation in predicting PIO remains a topic for future study.

The modified controller became progressively more sensitive as the feedback gains increased. Neither the low-gain set nor the medium-gain set exhibited PIO tendencies, and the desired criterion was generally met with both gain sets. For the low-gain set, using both fixed and motion-base simulation, pilot comments indicate that maneuver C had small amplitude oscillations of approximately 15 to 20 mrad, but the oscillations were easily eliminated by piloting technique. Maneuver A with motion had a slight pitch bobble of a few mrad, and maneuver D with motion had a small pitch oscillation.

For the medium gain set, maneuver B had a slight pitch sensitivity in both fixed and motion configurations. Maneuver C showed some overshoot tendency in the fixed-base configuration and a few more undesirable motions when the motion-base configuration was used. The test pilot found it difficult to excite the oscillations when he used maneuver D unless he was very aggressive.

For the high-gain set, motion had an effect during maneuver B and a small effect during maneuver D. During maneuver B with motion, a large amplitude PIO was obtained in both the longitudinal and lateral-direction axes, and the cause could not be distinguished; however, it was easy to excite the longitudinal controller. During maneuver C a full-stick deflection PIO was obtained in the fixed-base configuration, and divergent oscillations were obtained in the motion-base configuration. The pilot commented that he had to perform the task almost open loop. On maneuver D with motion, the pilot got into a low frequency PIO but commented that he probably could do the task and get desired performance without being aggressive.

One interesting point with the data in table 6 is that the modified controller with the high-gain set showed worse results than the baseline controller for maneuver D and comparable results for maneuver C and maneuver B under motion. One possible explanation is the order in which the experiments were done. The high-gain controller was evaluated last, two days after the baseline controller, and pilot fatigue could have influenced the results.

It appeared from the overall results that the low- and medium-gain sets would be satisfactory for flight, with the low-gain set slightly less sensitive. Desired performance was generally met with both gain sets. Both the baseline controller and the high-gain controller were very sensitive, and it was easy to generate PIO in maneuvers B and C. Use of motion resulted in only a very slight degradation with the baseline controller. These overall results are consistent with the Neal-Smith analysis.

## **Flight Results Summary**

This section contains a summary of the target-tracking results from the CY 1995 and 1996 flights. A more detailed presentation of the tracking results and results from all of the other maneuvers is presented in reference 6.

Thirteen pilots flew the HARV using the control system discussed in this paper. Six of these pilots provided ratings and comments. Letter designations have been given to all pilots (for consistency in reporting). The two project pilots who flew the baseline flight controller and most of the modified controller flights are referred to by letters D and E. Pilot E is also the pilot who flew the motion-based simulator in the United Kingdom. Data from the four guest pilots who flew some of the target-tracking tasks are combined, so letter notation is not important for them in this paper.

The fine target-tracking results showed the largest improvement of all maneuvers with the modified control system, when compared to the baseline flight results from CY 1994. In the CY 1994 flights, most tracking maneuvers could not be completed and were considered uncontrollable. In the CY 1995 and 1996 flights, all fine tracking maneuvers could be completed, although many runs were considered to still have pitch sensitivity. The average CHR and PIOR data for all target-tracking maneuvers are shown in table 7.

Pilot technique was found to have significant effect on target-tracking ratings. Pilot D used a moderately aggressive technique so that various points on the airplane would be tracked. Longitudinally, pilot D would track a point on the nose, aggressively move to track a point on the tail, and then repeat this procedure. In the lateral direction, pilot D moved from wing tip to wing tip several times. On average, level 1 to level 2 ratings were obtained, but there were undesirable motions (not PIO) that the pilot complained about.

Pilot E used a very aggressive approach, sort of like a “mini-acquisition” technique. In this technique the pilot moved off the target by a few reticule diameters and made a series of mini-acquisitions in

Table 7. Average Longitudinal CHR and PIOR Data for Target-Tracking Maneuvers

Target alpha, deg	Target Mach number	Gain set	Pilot D		Pilot E		Guest pilots	
			CHR	PIOR	CHR	PIOR	CHR	PIOR
30		Low	3.00	2	5.50	4.5	3.00	1
		Medium	3.75	3.33	6.33	4.67	3.14	1.5
		High	4.00	2				
45		Low	4.00	4	6.00	2.5		
		Medium	4.5	(a)	8.50	5	3.75	2.5
60		Medium	6.75		6.00	3.5		
	0.45	Medium	4.00					
	0.6	Medium			3.67			

<sup>a</sup>No PIOR because data are given for only 1 of 6 runs.

both the longitudinal and lateral-directional axes. Pilot E commented on several occasions that he could have tracked the target aircraft without difficulty, but he wanted to evaluate sensitivity. The theory is that any flight line pilot should be able to fly a control system without getting into a PIO. Ratings given by pilot E were much higher than those given by all other pilots. On average, level 2 to level 3 ratings were given, and the PIO ratings were generally in the PIO region.

Most guest pilots maintained smooth tracking of the target during the maneuver, and a couple of pilots also performed some mini-acquisitions. As shown in table 7, guest pilot ratings were borderline level 1, on average, with low sensitivity PIO ratings.

Postanalysis of the data showed that actuator rate limiting was a major reason for sensitivity (see ref. 6). Actuator rate limits were significantly exceeded during pilot E target-tracking flights, whereas linear actuator rate responses were generally observed during guest pilot flights. The degree of rate limiting observed indicates that sufficient nonlinearities were introduced into the control system to bring into question the results of the linear analysis previously presented.

## Conclusions

This paper describes the redesign and analysis of a Variable-Gain Output Feedback longitudinal controller that was flown on the High-Alpha Research Vehicle (HARV). Comparisons have been made for three gain sets that were evaluated in calendar year (CY) 1995 and 1996 flights. The feedback controller using the high-gain set was identical to that used in the baseline controller flown in CY 1994; therefore, feedback controller analysis that uses the high-gain set is also applicable to the baseline controller. The following list contains some of the main conclusions presented in the paper.

1. Single-loop Bode analysis shows that all design cases meet the specifications of 6-dB gain margin and 45° phase margin. Gain and phase margins generally increased with reduced integrator gain, particularly in the  $\alpha = 20^\circ$  to  $50^\circ$  range in which the greatest gain change occurred.

2. Loop transfer analysis shows that crossover frequencies for the high-speed cases are approximately twice that of the low-speed high-alpha cases. The high-speed case showed approximately the same response for all three gain sets. Comparison of the three gain sets for a low-speed high-alpha case shows a large gain reduction for the low-gain set at low frequencies and a slightly reduced crossover frequency.

3. Comparison of three gain sets for a structured singular value analysis shows that the low-gain set has improved robustness in the  $\alpha = 20^\circ$  to  $50^\circ$  range. The peak difference occurs at  $\alpha = 35^\circ$ , which is consistent with the design change.

4. A Neal-Smith flying qualities analysis shows that in the  $\alpha = 20^\circ$  to  $50^\circ$  range the high-gain set has a sensitivity problem and could have a tendency to pilot-induced oscillation (PIO). The low- and

medium-gain sets have significantly better results, with the low-gain set being slightly better than the medium-gain set. At a bandwidth of 3.0 rad/sec, the performance is just beyond the level 1 boundary, and at 3.5 rad/sec, the results are midway in the level 2 region.

5. A postflight analysis was made by using a recently developed high-alpha Bode envelope criterion. Frequency response data show that the magnitude of the closed-loop system is slightly high at  $1g$   $\alpha = 35^\circ$  but is within the proposed guidelines at loaded conditions. The magnitude of the low-gain set is improved over that of the high-gain set. Phase response data are within guidelines for all cases.

6. Results from simulation, both fixed-base and motion-base, show that the low- and medium-gain sets would be satisfactory for flight, with the low-gain set slightly less sensitive. Desired performance was generally met with both gain sets. Both the high-gain set and the baseline controller made the airplane overly sensitive to pilot input, thus the airplane was susceptible to PIO during target-tracking maneuvers. Motion generally resulted in a slight degradation of pilot ratings and the benefit of motion-based simulation in predicting PIO remains a topic for future study.

7. Fine-target-tracking flight results showed the largest improvement of all maneuvers with the modified control system when compared to the baseline flight results from CY 1994. Pilot technique had a significant effect on target-tracking ratings. Postanalysis of the data showed that actuator rate limiting was a major reason for sensitivity. The degree of rate limiting observed indicates that sufficient nonlinearities were introduced into the control system to bring into question the results of the linear analysis previously presented.

NASA Langley Research Center  
Hampton, VA 23681-2199  
December 1, 1997

## Appendix

### Variable-Gain Components and Modified Stochastic Weights

This appendix contains data (tables A1 through A4) showing the important changes from the data contained in reference 3 and is included in this paper for completeness. The first section contains the variable-gain components for each gain set, and the second section shows the modified stochastic weights used in the design algorithm. Reference 3 should be consulted for details on how to use these data.

#### Variable-Gain Components

This section contains data for the variable-gain matrix components (tables A1 through A3) that correspond to each of the three gain sets. Data for the high-gain set (table A1) are the same as in table VI in reference 3. Feedback gains can be calculated by inserting data from any of the following tables, along with appropriate trim conditions, into equation (24) in reference 3. In the table, the rows correspond to matrix components, and the columns correspond to the five outputs (three proportional outputs, one filter output, and one integrator output).

#### Modified Stochastic Weights

In reference 3, the stochastic weights for each of the five outputs were constant for all 39 design cases. The gain changes shown in tables A2 and A3 were obtained by adjusting the noise intensity on the integrator output (output 5) for design cases in the region of interest. One other adjustment was to assume high noise on the accelerometer output (output 3) to cause the load factor gains to be very small. This weight was changed from 0.01 to 1.0 for all 39 cases. Table A4 shows only the integrator stochastic weights.

Table A1. Components for High-Gain Set

Matrix components	$y_\alpha$	$y_q$	$y_{n_z}$	$y_u$	$y_z$
$\mathbf{K}_0$	-10.6285	-25.4721	-5.3189	21.9340	-30.8027
$\mathbf{K}_1$	-1.2185	-1.0865	-10.2974	-0.0423	-4.5770
$\mathbf{K}_2$	-3.5173	-12.7954	-18.7768	12.7372	14.6450
$\mathbf{K}_3$	4.4277	0.8839	0.2946	-6.7833	-16.0592
$\mathbf{K}_4$	33.5886	51.6908	38.9416	9.9597	-37.4526
$\mathbf{K}_5$	-1.5707	-0.6439	50.1606	1.7770	19.0618
$\mathbf{K}_6$	4.5668	9.1496	24.2615	1.5378	-8.7858

Table A2. Components for Medium-Gain Set

Matrix components	$y_\alpha$	$y_q$	$y_{n_z}$	$y_u$	$y_z$
$\mathbf{K}_0$	-14.6198	-21.7105	0	20.3047	-12.7707
$\mathbf{K}_1$	-1.4749	-1.2367	0	0.0709	-1.6904
$\mathbf{K}_2$	-2.4680	-16.2474	0	13.4838	2.1457
$\mathbf{K}_3$	3.4317	3.2854	0	-6.8320	-5.9890
$\mathbf{K}_4$	40.2194	53.0750	0	11.2317	-43.3383
$\mathbf{K}_5$	0.1742	-1.6711	0	1.9031	5.2069
$\mathbf{K}_6$	3.2383	13.2976	0	0.5205	3.7958

Table A3. Components for Low-Gain Set

Matrix components	$y_\alpha$	$y_q$	$y_{n_z}$	$y_u$	$y_z$
$K_0$	-17.3264	-19.2748	0	19.3828	-4.9819
$K_1$	-1.4839	-1.6110	0	0.2233	-0.4313
$K_2$	-1.5188	-17.5201	0	13.4916	-1.3299
$K_3$	2.3962	4.6838	0	-6.5514	-3.0343
$K_4$	42.8881	53.0575	0	12.3682	-43.0355
$K_5$	1.2616	-1.7377	0	1.5969	-0.5078
$K_6$	2.5020	14.3763	0	0.4619	4.9062

Table A4. Stochastic Weights on Integrator Output for Each Model

Model	High gain	Medium gain	Low gain
1	0.01	0.01	0.02
2	.01	.01	.02
3	.01	.01	.02
4	.01	.04	.08
5	.01	.04	.08
6	.01	.04	.08
7	.01	.005	.005
8	.01	.01	.02
9	.01	.01	.02
10	.01	.01	.02
11	.01	.04	.08
12	.01	.04	.08
13	.01	.04	.08
14	.01	.04	.08
15	.01	.01	.02
16	.01	.01	.02
17	.01	.04	.08
18	.01	.04	.08
19	.01	.04	.08
20	.01	.005	.005
21	.01	.01	.02
22	.01	.01	.02
23	.01	.01	.02
24	.01	.04	.08
25	.01	.04	.08
26	.01	.04	.08
27	.01	.04	.08
28	.01	.01	.02
29	.01	.01	.02
30	.01	.04	.08
31	.01	.04	.08
32	.01	.04	.08
33	.01	.005	.005
34	.01	.01	.02
35	.01	.01	.02
36	.01	.01	.02
37	.01	.04	.08
38	.01	.04	.08
39	.01	.04	.08

## References

1. Halyo, Nesim; Moerder, Daniel D.; Broussard, John R.; and Taylor, Deborah B.: *A Variable-Gain Output Feedback Control Design Methodology*. NASA CR-4226, 1989.
2. Ostroff, Aaron J.; and Proffitt, Melissa S.: *Longitudinal-Control Design Approach for High-Angle-of-Attack Aircraft*. NASA TP-3302, 1993.
3. Ostroff, Aaron J.; Hoffler, Keith D.; Proffitt, Melissa S.: *High-Alpha Research Vehicle (HARV) Longitudinal Controller: Design, Analyses, and Simulation Results*. NASA TP-3446, 1994.
4. Davidson, J. B.; Foster, J. V.; Ostroff, A. J.; Lallman, F. R.; Murphy, P. C.; Hoffler, K. D.; and Messina, M. D.: Development of a Control Law Design Process Utilizing Advanced Synthesis Methods With Application to the NASA F-18 HARV. *The Compton Observatory Science Workshop*, Chris R. Shrader, Neil Gehrels, and Brian Dennis, eds., NASA CP-3137, vol. 4, 1992, pp. 111–157.
5. Matheny, Neil W., compiler: *High-Angle-of-Attack Projects and Technology Conference*. NASA CP-3137, 1992.
6. Ostroff, Aaron J.; and Wichman, Keith D.: Flight Evaluation of Variable-Gain Output Feedback Longitudinal Control Law for the NASA F/A-18 High Alpha Research Vehicle (HARV). Presented at the *High-Angle-of-Attack Technology Conference* (Langley Research Center, Hampton, VA), Sept. 17–19, 1996.
7. Pahle, Joseph W.; Bundick, W. Thomas; Yeager, Jessie C.; and Beissner, Fred L., Jr.: *Design of a Mixer for the Thrust-Vectoring System on the High-Alpha Research Vehicle*. NASA TM-110228, 1996.
8. Broussard, J. R.: *Design, Implementation and Flight Testing of PIF Autopilots for General Aviation Aircraft*. NASA CR-3709, 1983.
9. Maybeck, Peter S.: *Stochastic Models, Estimation and Control*. Academic Press, 1982.
10. Neal, T. P.; and Smith, R. E.: An In-Flight Investigation to Develop Control System Design Criteria for Fighter Airplanes, Volume 1. AFFDL-TR-70-74-VOL-1, U.S. Air Force, 1970.
11. Wilson, David J.; and Citurs, Kevin D.: High Angle of Attack Flying Qualities Design Guidelines. NASA CR-4681, vol. 1–2, 1996.
12. Hoffler, Keith D.; Brown, Philip W.; Phillips, Michael R.; Rivers, Robert A.; Davidson, John B., Jr.; Lallman, Frederick J.; Murphy, Patrick C.; and Ostroff, Aaron J.: Evaluation Maneuver and Guideline Development for High-Alpha Control Law Design Using Piloted Simulation. AIAA-94-3512, Aug. 1994.
13. Cooper, G. E.; and Harper, R. P., Jr.: *The Use of Pilot Rating in the Evaluation of Aircraft Handling Qualities*. NASA TN D-5153, 1969.
14. Wichman, Keith D.; Pahle, Joseph W.; Bahm, Catherine; Davidson, John B.; Bacon, Barton J.; Murphy, Patrick C.; Ostroff, Aaron J.; and Hoffler, Keith D.: *High-Alpha Handling Qualities Flight Research on the NASA F/A-18 High Alpha Research Vehicle*. NASA TM-4773, 1996.
15. White, A. D.; Hall, J. R.; and Tomlinson, B. N.: Initial Validation of a R/D Simulator With Large Amplitude Motion. *Piloted Simulation Effectiveness*, AGARD CP-513, 1992.
16. Krekeler, Gregory C., Jr.; Wilson, David J.; and Riley, David R.: High Angle of Attack Flying Qualities Criteria. AIAA-90-0219, 1990.
17. Wilson, David J.; and Riley, David R.: *Flying Qualities Criteria Development Through Manned Simulation for 45° Angle of Attack—Volumes 1 and 2: Simulation Results and Analysis*. NASA CR-4435, 1992.

